Pergamon

Geochimica et Cosmochimica Acta, Vol. 67, No. 3, pp. 325–343, 2003

0016-7037/03 $22.00 + .00

PII S0016-7037(02)00965-1

A method for precise measurement of argon 40/36 and krypton/argon ratios in trapped air in polar ice with applications to past firn thickness and abrupt climate change in Greenland and at Siple Dome, Antarctica

JEFFREY P. SEVERINGHAUS,[1,*] ALEXI GRACHEV,[1] BOAZ LUZ,[2] and NICOLAS CAILLON[3]

[1]Scripps Institution of Oceanography, University of California San Diego, La Jolla, CA 92093, USA
[2]The Institute of Earth Sciences, The Hebrew University of Jerusalem, Jerusalem 91904, Israel
[3]IPSL Laboratoire des Sciences du Climat et de l'Environnement, UMR CEA-CNRS 1572, CEA Saclay, 91191 Gif-sur-Yvette, France

(*Received September* 18, 2001; *accepted in revised form May* 10, 2002)

Abstract—We describe a method for measuring the $^{40}Ar/^{36}Ar$ ratio and the $^{84}Kr/^{36}Ar$ ratio in air from bubbles trapped in ice cores. These ratios can provide constraints on the past thickness of the firn layer at the ice core site and on the magnitude of past rapid temperature variations when combined with measured $^{15}N/^{14}N$. Both variables contribute to paleoclimatic studies and ultimately to the understanding of the controls on Earth's climate. The overall precision of the $^{40}Ar/^{36}Ar$ method (1 standard error of the mean) is 0.012‰ for a sample analyzed in duplicate, corresponding to ±0.6 m in reconstructed firn thickness. We use conventional dynamic isotope ratio mass spectrometry with minor modifications and special gas handling techniques designed to avoid fractionation. About 100 g of ice is used for a duplicate pair of analyses. An example of the technique applied to the GISP2 ice core yields an estimate of 11 ± 3K of abrupt warming at the end of the last glacial period 15,000 years ago. The krypton/argon ratio can provide a diagnostic of argon leakage out of the bubbles, which may happen (naturally) during bubble close-off or (artifactually) if samples are warmed near the freezing point during core retrieval or storage. Argon leakage may fractionate the remaining $^{40}Ar/^{36}Ar$ ratio by +0.007‰ per ‰ change in $^{84}Kr/^{36}Ar$, introducing a possible bias in reconstructed firn thickness of about +2 m if thermal diffusion is not accounted for or +6 m if thermal diffusion effects are quantified with measured $^{15}N/^{14}N$. Reproducibility of $^{84}Kr/^{36}Ar$ measured in air is about ±0.2‰ (1 standard error of the mean) but is about ±1‰ for ice core samples. Ice core samples are systematically enriched in $^{84}Kr/^{36}Ar$ relative to atmosphere by ~5‰, probably reflecting preferential size-dependent exclusion of the smaller argon atom during bubble entrapment. Recent results from the Siple Dome ice core reveal two climate events during the last deglaciation, including an 18-m reduction in firn thickness associated with an abrupt warming at sometime between 18 and 22 kyr BP and a partial or total removal of the firn during an ablation event at 15.3 kyr BP.

1. INTRODUCTION

Measurements of stable isotopes of inert or near-inert gases trapped in air bubbles in ice cores have been used to infer ancient environmental conditions at the surface of ice sheets, adding to understanding of the controls on Earth's climate (Sowers et al., 1989, 1992; Craig and Wiens, 1996; Severinghaus et al., 1998; Severinghaus and Brook, 1999; Lang et al., 1999; Leuenberger et al., 1999; Caillon et al., 2001). Argon has three stable isotopes, argon-40, argon-38, and argon-36, whose atmospheric ratios are highly constant on time scales of 10^5 yr. Variations observed in these ratios in trapped air in ice thus must arise locally in the porous layer of snow (firn) at the surface of the ice sheets from processes associated with the entrapment of air. Diffusive separation of the isotopes is possible in the stagnant layer of air in porous firn by two physical processes: gravitational settling and thermal diffusion. The amount of isotope fractionation by gravitational settling increases with depth in a known way in the stagnant (diffusion-dominated) portion of the firn, as given by the barometric equation (Craig et al., 1988; Schwander, 1989; Sowers et al., 1989): $\delta = [e^{\Delta mgz/RT} - 1]10^3$‰, where δ is the isotopic deviation (defined in Eqn. 1), Δm is the mass difference between the isotope pair, g is gravitational acceleration, z is depth, R is the gas constant, and T is temperature. For example, the air at the bottom of a 92-m deep stagnant air column at 226K will be enriched by +1.92‰ in $^{40}Ar/^{36}Ar$ ($\delta^{40}Ar$) relative to the top of the column (in our case, the atmosphere). The closing bubbles trap air at the bottom of the firn layer, so the bubble-air isotopes can provide a record of past diffusive column thickness. The diffusive column thickness in turn is affected by absolute temperature, snow accumulation rate, and possibly wind speed (Sowers et al., 1989, 1992), and paleo-thickness estimates can provide constraints on these variables when combined with other information.

Thermal diffusion fractionation reflects the presence of temperature gradients in the ancient firn (Severinghaus et al., 1998; Severinghaus and Brook, 1999). Immediately following an abrupt temperature change at the surface, a temperature gradient exists in the firn temporarily due to the thermal inertia of the underlying firn and ice. This temperature gradient causes gas isotopes to separate, with heavier isotopes migrating toward cooler regions (Grew and Ibbs, 1952). The amount of thermal diffusion fractionation is given by $\delta = \Omega^{X/Y}\Delta T$, where ΔT is the temperature difference between the top and bottom of the

* Author to whom correspondence should be addressed (jseveringhaus@ucsd.edu).

diffusive column and $\Omega^{X/Y}$ is the "thermal diffusion sensitivity." This is an empirical quasi-constant characteristic of gas pair X/Y, which is measured in the laboratory by equilibrating air in a known temperature gradient and measuring the fractionation. For the pair ^{40}Ar-^{36}Ar in air at a mean temperature of 230K, $\Omega^{40/36}$ (denoted Ω^{40} for brevity) is about $+0.039‰\ K^{-1}$ (Grachev and Severinghaus, 1999; Severinghaus et al., 2001). For example, a 10-K temperature difference will cause a $+0.39‰$ enrichment of δ^{40}Ar in the cold gas relative to the warm gas. These isotopic anomalies diffuse down to the bubble close-off region (at a rate 10× faster than the heat diffuses) and so are preserved in the air bubbles in the ice. The effect of gravitational settling may be removed by measuring both δ^{40}Ar and the ^{15}N/^{14}N ratio of N_2 (δ^{15}N), because argon isotopes are less sensitive to thermal diffusion than nitrogen isotopes, as discussed below. With the help of a heat transfer model of the firn, the anomaly magnitudes provide a direct estimate of the magnitude of abrupt climatic warming or cooling at the surface of the ice sheet in the past (Severinghaus et al., 1998; Severinghaus and Brook, 1999). Furthermore, the fact that the temperature signal is borne by a gas circumvents the troublesome issue of the gas age-ice age difference and allows for the first time a precise comparison of the timing of atmospheric gas variations such as methane relative to the temperature event (Severinghaus et al., 1998).

The signals associated with these processes are rather small, however, demanding an order-of-magnitude increase in measurement precision compared to previous measurements. Our experience has shown that it is easy to accidentally fractionate the isotopes at this level of precision during gas handling, requiring the development of special gas-handling techniques that minimize fractionation. Here we describe a method for extracting the noble gases and measuring deviations in the ^{40}Ar/^{36}Ar and ^{84}Kr/^{36}Ar ratios with conventional isotope ratio mass spectrometry, which gives sufficient precision for meaningful paleoenvironmental application. We then show examples of applications from the GISP2 (Greenland) and Siple Dome (West Antarctica) ice cores, where firn thickness through time and the magnitude of a discrete abrupt warming event are estimated.

2. EXTRACTION OF NOBLE GASES FROM ICE

We employ a wet extraction technique that was developed at the University of Rhode Island in the Bender Laboratory, based partly on the technique of Sowers et al. (1989). Ice samples weighing approximately 45 g are cut from hand samples obtained from the National Ice Core Laboratory in Denver, Colorado. A band saw in a walk-in freezer at −20°C is used to cut the samples and trim all faces, removing at least 0.5 cm of ice to expose fresh surfaces. Dimensions of the piece are ~2.3 × 2.3 × 9 cm, with the long axis oriented parallel to the ice core so as to average over several annual layers. The piece is further cut in two to fit in the extraction vessel. The extraction vessels are constructed of a stainless steel Conflat vacuum fitting with a glass-to-metal transition and a custom-made glass vessel with total volume of ~400 cm^3 (Fig. 1).

Ice samples are lowered with chilled tongs into prechilled extraction vessels in a small top-opening freezer. The vessels contain a glass-covered magnetic stir bar to agitate the meltwater. The vessels are immersed in ethanol at −20°C to keep

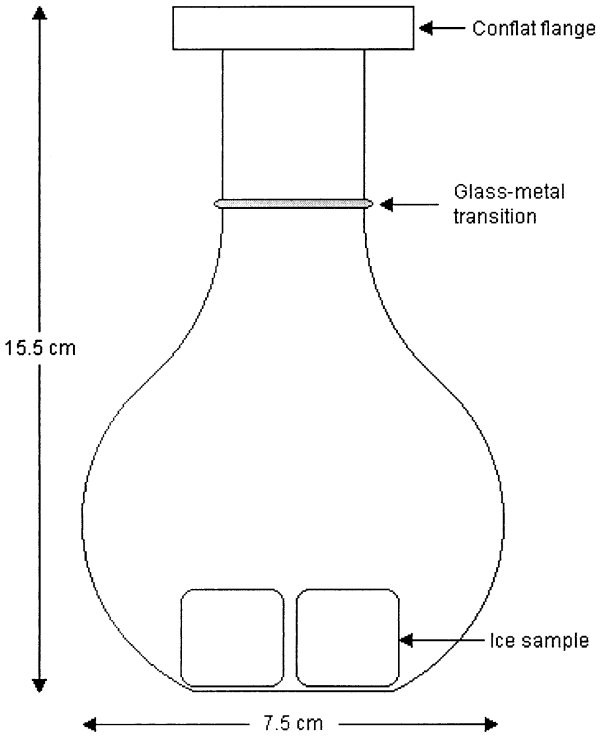

Fig. 1. Vacuum extraction vessel with ice sample inside. Note that the ice is kept as far away as possible from the (warm) stainless steel fitting at the top by carefully laying the ice samples on their sides at the bottom of the vessel. This minimizes warming of the ice, which may cause leakage of the trapped gas during evacuation.

them cold during the pumpdown. Copper gaskets are used only twice to make the Conflat seal. We had previously used the gaskets up to 10 times to reduce cost but had problems after a change of gasket manufacturer, with leaks attributed to work-hardening of the copper. The vessels containing ice are bolted on to the vacuum line, minimizing the time spent out of the cold ethanol. The room air is then evacuated from the vessels for 40 min at −20°C. Typically, two or three samples are simultaneously evacuated to speed the process. The vapor pressure over ice at −20°C is considerable (100 Pa), so a continual flux of sublimed vapor aids in the sweep-out of the room air. Sublimation also cleans the surface of the ice sample of any adsorbed air. Care is taken to insure that the temperatures of the different ethanol dewars are similar so that the vapor pressures in the different vessels will be similar. The vacuum is provided by a turbomolecular pump (Balzers) backed by a rotary vane "rough" pump (Alcatel), and background pressures are typically ~10^{-3} Pa as measured on a Bayert-Alpert-type ion gauge (Granville-Phillips).

After evacuation, the vessels are sealed and warmed to room temperature (21°C), releasing the trapped gas by melting. Gases are transferred to a collection vessel at 10K for 15 min to obtain quantitative transfer. On the way, the gas passes through a water trap at −100°C via a capillary, in effect using water vapor as a carrier gas to improve sweep-out of the sample from the large vessel (Fig. 2). The melt is agitated vigorously with the magnetic stirrer. We found that gentle stirring was not sufficient to obtain complete extraction of the gases, which may

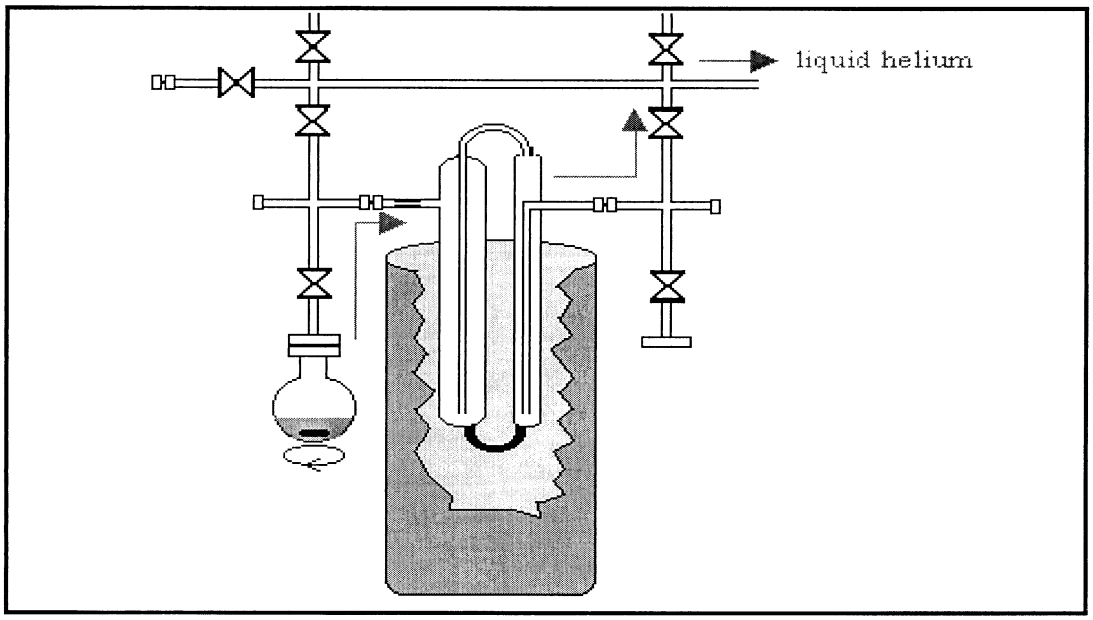

Fig. 2. Wet extraction apparatus using the water vapor as a carrier gas, with flow through a 0.7-mm ID capillary 3-cm long to retard the flow of water vapor. Hot Pyrex water trap is flushed with dry air before attaching it to the rack to speed pumpdown. Ultratorr fittings used to connect trap to rack are drilled out to allow fittings to slide completely over Pyrex tubing, permitting trap to be inserted in a short gap in the rack.

be important for the very soluble gases such as Xe. After passing through the water trap, the gas is frozen at 10K (in a dewar of liquid helium) in the stainless steel collection vessel, which is made of a 70-cm long, 1/4″ diameter tube. The vessel is lowered into the liquid helium in three stages over the course of the transfer to improve the freeze-down of the gas by exposing fresh metal surfaces. Residual pressure is checked using a convectron gauge (Granville-Phillips) after the 15 min transfer is over. High residual pressure can indicate incomplete transfer and is used as a basis for rejection of a sample. The yield of gas is approximately 4 standard cm^3.

The gas is then exposed to a Zr/Al (SAES) getter in a quartz oven (Fig. 3) to absorb the N_2, O_2, and other reactive gases. The getter material is an alloy of Zr and Al that is provided by the manufacturer in small "sheets," and four getter sheets are used per sample. The getter is prepared by 5 min of evacuation at 100°C followed by activation by heating at 900°C under vacuum for 5 min. The sample is gettered for 10 min at 900°C, followed by an additional 2 min at 300°C to remove H_2 gas. The oven is turned off, the sample is released, and pressure is recorded with a capacitance manometer (MKS). The mixture of noble gases is then frozen into a second stainless steel vessel at 10K for 3 min. Ultrahigh purity tank N_2 equal to 10× the noble gas pressure is then added to the sample to give it more bulk (sample bulk is needed to maintain the pressure in the mass spectrometer capillaries within the viscous flow regime). This N_2 is transferred to the same vessel at 10K for another 3 min. The mixture is warmed to room temperature and allowed to homogenize for 40 min before mass spectrometric analysis. The resulting mixture contains ~0.4 cm^3 (STP) of gas.

3. MASS SPECTROMETRY

Isotopic ratios are analyzed on a dual viscous-inlet Finnigan MAT 252 mass spectrometer at the Scripps Institution of Oceanography (SIO) equipped with Faraday cups in the appropriate positions for simultaneous collection of ^{40}Ar and ^{36}Ar beams. This type of machine differs from those typically used to measure noble gases in that it is a dynamic-inlet instrument that uses far more sample (on the order of 1 cm^3 STP). Precision is attained by bleeding sample and standard gases through two capillaries that are alternately fed into the mass spectrometer or into a waste line at high vacuum, with rapid switching between sample and standard minimizing the effect of instrument drift (McKinney et al., 1950). Minor modifications to this commercially available instrument were made to increase precision, as described below.

The routine analysis is performed as follows. The sample mixture is expanded into the fully open sample bellows of the mass spectrometer inlet and is allowed to equilibrate for 3 min to homogenize. Because the bellows volume is ~40 cm^3 and the stainless vessel volume is ~10 cm^3, only ~4/5 of the sample makes it into the bellows for analysis. Thus, there is a possibility of fractionating the sample at this step, and we will return to this topic. A similar expansion is made into the standard bellows of an aliquot of standard gas prepared from commercial tank N_2, Ar, and Kr in appropriate proportions. Typical pressures on expansion are ~800 Pa. Valves are closed, and both bellows are compressed to 3800 Pa, our nominal running pressure at the beginning of an

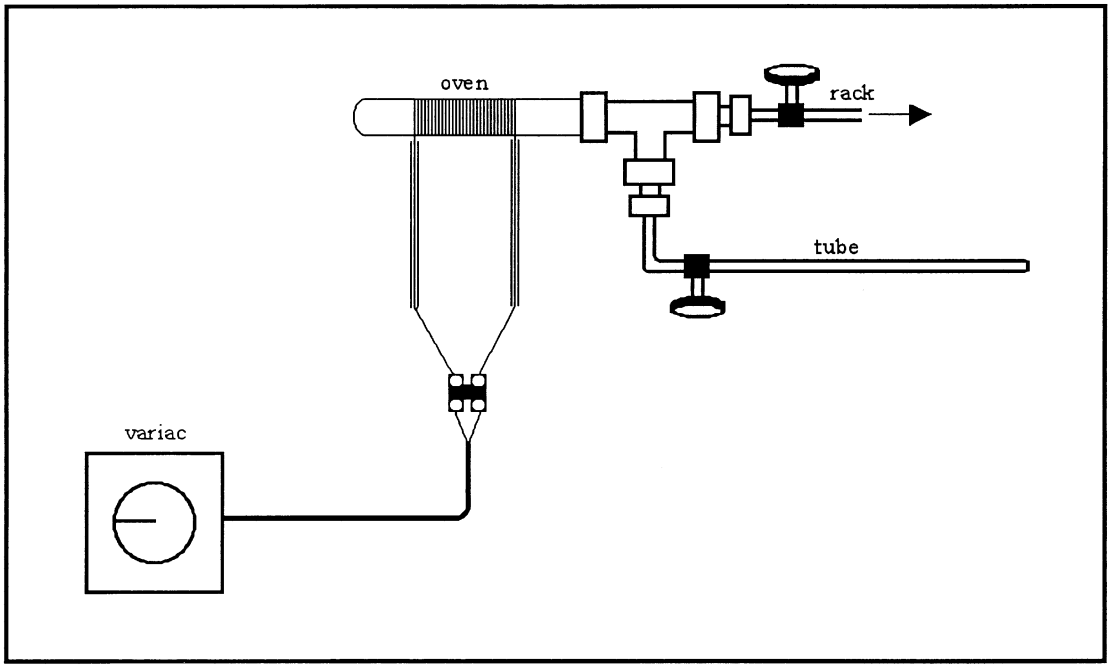

Fig. 3. Experimental setup for gettering. Oven is made from 1/2″ OD quartz tube wrapped with INCONEL heating wire, powered by 120 V AC modulated by a Variac. Ultratorr tee (1/2″) is used to connect stainless tube containing the sample to the getter oven.

analysis (at the end of the $^{40}Ar/^{36}Ar$ analysis, pressures are ~3600 Pa).

Beam currents are typically 2×10^{-9} amps for ^{40}Ar and 6×10^{-12} amps for ^{36}Ar, corresponding to ~2 V on 1×10^{9} ohm (^{40}Ar) and 3×10^{11} ohm (^{36}Ar) resistors (a preamplifier converts each beam current into a voltage between 0 and 10 V DC). Sample and standard beam voltages are balanced by manually adjusting the bellows pressure. Because sample and standard quantities of gas are usually a little different, the rate of pressure fall differs between the two sides as the gas is depleted in each bellows, making pressures become unbalanced during the run. The side having less gas is therefore started off a little high, so that it will equal the other side halfway through the run. The beam voltages V^{40} and V^{36} are simultaneously integrated for 8 s on standard, sample, and then standard sides, constituting one "cycle." After switching between standard and sample, a delay of 10 s is allowed before acquisition of data to permit the beam to stabilize. The two standard measurements in a cycle are averaged to normalize for instrument drift. A δ value is then calculated for each cycle according to:

$$\delta^{40}Ar \equiv [(^{40}Ar/^{36}Ar_{sample})/(^{40}Ar/^{36}Ar_{standard}) - 1]10^{3}‰ \quad (1)$$

where $^{40}Ar/^{36}Ar = (V^{40} - B^{40})/(V^{36} - B^{36})$. The constant B is an extremely small background voltage assigned to each Faraday cup that is measured by closing the mass spectrometer to both standard and sample gas streams, waiting 60 s, then integrating the residual voltage for 8 s. Backgrounds are only run at the beginning of a set of measurements (once a month or so), and the same value of B is used throughout the set of measurements.

The resulting δ value is expressed in ‰ units. A "block" is defined as a group of cycles, in our case 16 cycles, at the beginning of which a "peak centering" is done to position the beam in the center of the Faraday cup. We run three consecutive blocks to obtain 48 cycles over a ~35-min period. At the end of each block, rejection of outliers is done automatically by the ISODAT software using a Dixon outlier test (risk level D3 corresponding to the 90% confidence level). The mean δ of the remaining cycles is reported, with a typical standard deviation of the individual δs from the mean of ~0.07‰. Thus, the nominal internal precision of the measurement, expressed as a standard error of the mean, would be $0.07‰/(48)^{0.5} = 0.01‰$. Beam voltage is recorded by the ISODAT software at the beginning of each block, which we use to make post measurement corrections for pressure imbalance.

3.1. Pressure Imbalance Correction

The measured δ value is slightly sensitive to differences in the pressure in the two bellows, requiring a small correction. This correction involves measuring the pressure imbalance sensitivity (PIS) weekly, which is done by grossly unbalancing sample and standard sides (by ~10%), running four cycles, and recording the resulting δ (called $\delta_{unbalanced}$) and beam current imbalance Δ_P for a sample with a known value δ_{true}:

$$PIS \equiv [\delta_{unbalanced} - \delta_{true}]/\Delta_P \quad (2)$$

where $\Delta_P \equiv \{[V_{sample}/V_{standard} - 1]10^{3}‰\}$. The pressure imbalance sensitivity can change with adjustments to the source

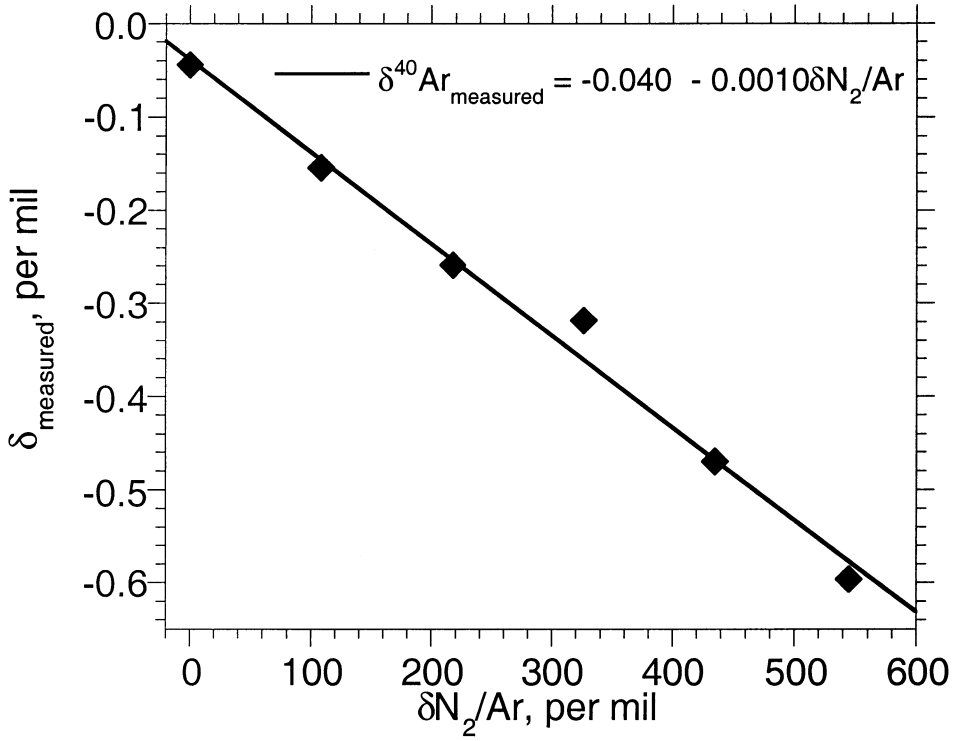

Fig. 4. Empirical determination of the "chemical slope" by adding increasing amounts of pure nitrogen gas to aliquots of the standard gas, which is composed of argon and N_2. The chemical slope is found by regression of the resulting observed δs.

parameters (electron energy and trap voltage) and the settings for beam focusing, and it is likely to be closely related to the nonlinearity of the mass spectrometer. The pressure imbalance correction is made to unknown samples by assuming that (1) the pressure imbalance-related δ deviation varies linearly with pressure imbalance, which is supported by experiments (Bender et al., 1994a) and (2) by assuming that the PIS is stable over time (at least for a week or so). The correction is as follows:

$$\delta_{\text{pressure corrected}} \equiv \delta_{\text{measured}} - (\text{PIS})\ \Delta_P \qquad (3)$$

The average pressure imbalance Δ_P during the entire run is calculated from the recorded beam voltages at the beginnings of the first and third blocks. These are interpolated in time to the midpoint of the second block, which is the midpoint of the entire run. Typical values of PIS are −0.001‰/‰, and the pressure imbalance is usually <5‰, so the correction is generally <0.005‰. It is worth noting that we have seen much larger PIS (factor of 100 greater) when the background has not been updated following a change of resistor or a change of gas type. This is explainable as being due to the fact that subtraction of an inappropriate (and constant) value of *B* from both numerator and denominator of the voltage ratio will create spurious variation in the δ if standard and sample voltages are not equal (i.e., if there is any pressure imbalance).

3.2. Chemical Slope Correction

Mixtures of gases present an additional complication to mass spectrometry. Measured isotopic ratios of a single element in a mixture of gases are generally sensitive to variations in the elemental ratios of the mixture. The relative ionization efficiencies of ^{40}Ar and ^{36}Ar in the mass spectrometer source are affected by differences in sample and standard N_2/Ar ratios, probably due to charge transfer between Ar and N_2 in the source (Kurt Marti, 2001, pers. comm.). We call this type of sensitivity the "chemical slope," and this requires a correction based on the measured N_2/Ar ratio of the sample and a prior experimental determination of the chemical slope. The chemical slope is measured periodically (typically at the start of a major set of measurements lasting a month or a few months) by adding progressively increasing amounts of pure N_2 to aliquots of standard gas and running them against the standard gas. Since the true argon isotope ratios are identical in sample and standard in this case, any observed deviation in $\delta_{\text{pressure corrected}}$ must be due to the chemical slope (Fig. 4). The chemical slope correction is applied to unknown samples according to:

$$\delta^{40}Ar_{\text{slope corrected}} \equiv \delta_{\text{pressure corrected}} - [\text{chemical slope}]\ \delta N_2/Ar_{\text{measured}} \qquad (4)$$

A typical value for the chemical slope of $\delta^{40}Ar$ on the SIO machine is −0.001‰/‰. The $\delta N_2/Ar$ values are in almost all cases <10‰, meaning that the chemical slope correction is almost always <0.01‰. We measure $\delta N_2/Ar$ in a single collector with the Interfering Masses program of ISODAT software, which periodically varies the magnetic field ("peak jumping"). We make four measurements in a sequence: sample mass 29, standard mass 29, sample mass 40, and then standard mass 40. The $\delta N_2/Ar$ is calculated as:

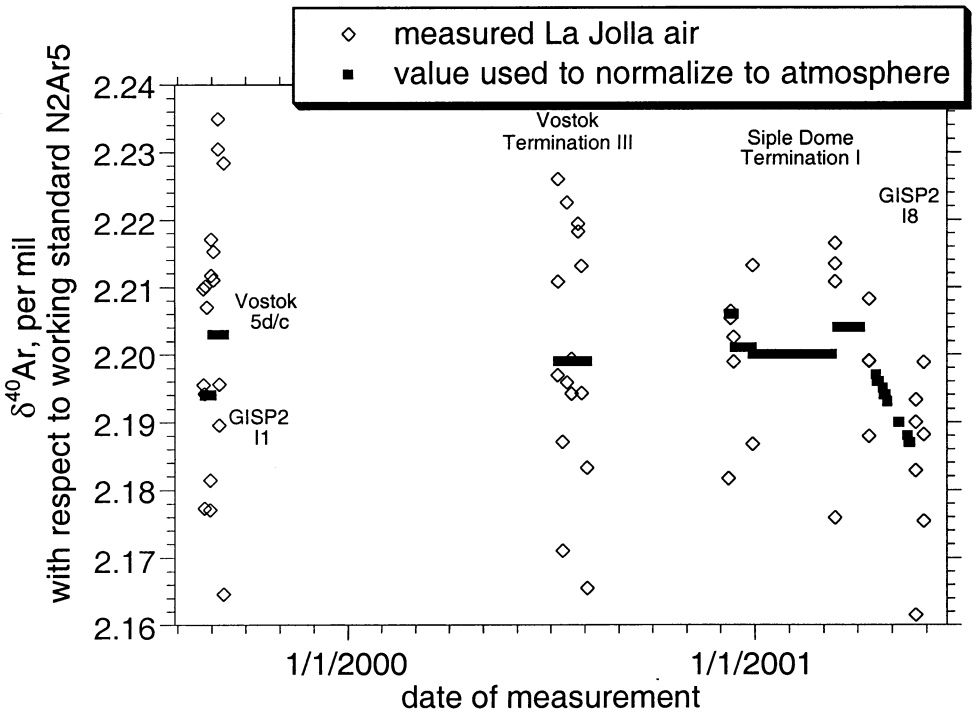

Fig. 5. Repeated measurements of δ^{40}Ar in La Jolla air (obtained from the outside of the lab building) vs. the working standard gas N2Ar5 over a 2-yr period. A solid square is shown for each ice sample run, giving the value of La Jolla air that was used to normalize the ice core data to the ultimate atmospheric ratio reference.

$$\delta N_2/Ar = [(V^{29}/V^{40}_{sample})/(V^{29}/V^{40}_{standard}) - 1]10^3‰ \quad (5)$$

It should be noted that different machines can have very different chemical slopes. For example, a machine at the University of Rhode Island had a chemical slope for δ^{18}O of O_2 in air that was 22× that of the SIO machine. Changes in the source parameters can affect the chemical slope, and it can even change sign in response to source tuning. The SIO machine is tuned to optimize linearity, and it is likely that this minimizes the chemical slope. This optimum is found by adjusting the ion extraction potentiometer while noting the voltage of a given beam. The voltage has two maxima, one being much lower than the other, and the optimum linearity is found by setting the ion extraction to this secondary peak.

3.3. Normalization to Atmosphere

The atmosphere is the ultimate standard gas to which all our measurements are referred. Our working standard gas, however, is made from pure tank Ar and N_2, and the isotopes of these gases are highly fractionated with respect to atmosphere due to the commercial air reduction process. Thus, a normalization to the data is necessary to express the results with respect to atmosphere. We make this normalization by measuring aliquots of 4 cm^3 (STP) of dry air taken from the exterior of the laboratory building, which we call La Jolla air. The technique for sampling the air follows loosely that of Keeling et al. (1998). La Jolla air is dried by pumping it at 5 L min^{-1} through two sequential glass water traps at −100°C (ethanol dewar), with 3-mm diameter glass beads in the traps to improve surface contact of the water molecules. The pump (KNF Neuberger Teflon diaphragm) is modified to improve the seal on the head gasket by installing a viton O-ring in a machined groove in the aluminum head. Tubing used is 1/4″ OD Dekabon polyethylene-aluminum composite tubing, and connections are made with Ultratorr fittings having Viton O-rings. A 2-L glass flask is placed downstream of the pump to reduce pressure fluctuations caused by the pump, and two 4-cm^3 sample volumes are placed downstream of the flask. A tail of 2 m of tubing is attached to the downstream end of the sample volumes to prevent wet air from getting into the sample volume. The assembly is flushed for 10 min without changing the thermal environment of the water traps to insure that a steady state has been reached in which the air in the sample volume is an unfractionated sample of the atmosphere. Then the pump is stopped, and the sample valves are closed after 5 s to allow airflow to cease. Care is taken to avoid temperature gradients in the vicinity of the sample volume, as thermal fractionation is a potential issue even at these high flow rates (Manning, 2001).

The La Jolla air sample is run through the same procedure as ice core samples, mimicking as closely as possible the path taken by ice core samples. Slope and pressure corrections are made as for ice core samples. Thus, any small fractionation or contamination imposed on the samples will also be imposed on the La Jolla air and will cancel to first order. Over a 2-yr period, 59 measurements of La Jolla air vs. the working standard N2Ar5 were made (Fig. 5). Four measurements were rejected based on identified leaks and other methodologic problems. The remaining 55 measurements had a mean value of

+2.199‰ and a standard deviation of 0.017‰. This latter value serves as one (conservative) measure of the long-term external precision. The fact that this value is slightly larger than the internal precision may reflect additional variance due to gas handling or drift in the mass spectrometer or standard gas over time. The principle used in normalizing the ice core samples to atmosphere is to try to find the best estimate of La Jolla air $\delta_{40}Ar_{\text{La Jolla air}}$, during the period in which the ice core samples were measured, and normalize as follows:

$$\delta^{40}Ar_{\text{normalized}} \equiv (\{[\delta^{40}Ar_{\text{slope corrected}}]/1000 + 1\}/\{[\delta^{40}Ar_{\text{La Jolla air}}]/1000 + 1\} - 1)10^3‰ \quad (6)$$

Two to four replicate analyses of La Jolla air are made on one day, typically at the start of a set of measurements, and further sets of two to four analyses are made at roughly weekly intervals and at the end of a set of measurements. An assessment is made of the possibility of significant change in the values over the course of the set of measurements. This could be due to drift in the mass spectrometer or standard gas (for example, due to slight fractionation of the standard gas by leaking through the small orifice of an incompletely closed valve). Significance is determined by a t-test, assuming that the true standard deviations do not vary (the typical standard deviation of a set of four La Jolla air measurements made on the same day is 0.012‰). If there is no significant change, the mean of all the La Jolla air analyses done during that particular set of measurements is used to normalize the ice core data. The Vostok and Siple Dome sets of measurements fall into this category (Fig. 5).

On the other hand, if there is significant change, then a linear interpolation of $\delta^{40}Ar_{\text{La Jolla air}}$ in time is made between the two differing values, and this interpolated value is used to normalize the ice core data based on the date of measurement. The justification for this approach is that a drift in the standard gas, if it occurred, would likely be gradual and thus well approximated by a linear interpolation in time (although we cannot rule out a "step" change that occurred all at once). The GISP2 I8 set is an example of this second category (Fig. 5) as follows. At the beginning of this set on April 11, 2001 (Fig. 5), La Jolla air had a value of 2.199 ± 0.008‰ (1 standard deviation, $n = 4$). La Jolla air was not measured again until May 26, 2001, at the end of the set of measurements. At this time, it was 2.184 ± 0.013‰ (1 standard deviation, $n = 7$). Pooling the standard deviations resulted in a value of 0.012‰ (degrees of freedom = 9), which via a t-test gave the result that the difference was not significant at the 95% confidence level. However, it was significant at the 90% confidence level, and in our judgment this was sufficient for the purposes of making a small correction. Thus, we concluded that a drift had occurred, triggering the linear downward trend in the value used to normalize (Fig. 5).

3.4. Reproducibility of Ice Measurements

A second measure of the external precision is the ability to reproduce an ice core measurement, where the ice is all cut from the same depth in the ice core and thus arguably should have the same true isotope composition. We obtained some GISP2 Holocene ice that had been accidentally warmed to the melting point and thus rendered unusable for paleoclimatic purposes (near the melting point, gases leak out of glacial ice and have been shown to fractionate the remaining gases). A sample of this "practice" ice from 687.25- to 687.45-m depth was run eight times and gave a standard deviation of 0.017‰, and another piece from 517.08 to 517.28 m was also run eight times and gave a standard deviation of 0.016‰.

Because we run all ice core samples in duplicate or triplicate, the deviation of replicates from each other can also give information about reproducibility. We define the pooled standard deviation s_{pooled} as the square root of the summed squared deviations of replicates δ_i from their respective means, divided by the degrees of freedom (the number of samples n minus the number of reported means m):

$$S_{pooled} \equiv \left(\frac{\sum_{i,j=1}^{n,m} (\delta_i - \overline{\delta}_j)^2}{n - m} \right)^{0.5} \quad (7)$$

For example, the GISP2 I1 (Bølling) data set has $n = 28$, $m = 14$, and $s_{\text{pooled}} = 0.021$‰. This was an early effort, and precision was lower due to our learning. The GISP2 I8 set has $n = 48$, $m = 24$, and $s_{\text{pooled}} = 0.012$‰. The Siple Dome set has $n = 175$, $m = 87$, and $s_{\text{pooled}} = 0.021$‰. The reason for the greater scatter in the Siple Dome samples is not clear but could be due to the fact that the core is extensively fractured and contaminated with butyl acetate, the drilling fluid used (which could be smelled in Siple Dome samples but not in others). The Vostok Termination III set has $n = 112$, $m = 56$, and $s_{\text{pooled}} = 0.013$‰.

Taking a value of 0.017‰ as representative of our standard deviation, the standard error of an ice sample analyzed in duplicate (as we typically do) is $0.017/2^{0.5} = 0.012$‰. For comparison, the typical thermal diffusion signals associated with abrupt climate change in the Greenland ice cores are about +0.4‰, giving a signal-to-noise ratio of ~30. Gravitational signals are typically +2‰, giving a signal-to-noise ratio of ~160. During periods of constant climate, when thermal diffusion can be safely neglected, this error corresponds to an uncertainty in the reconstructed firn diffusive column thickness of ~0.6 m. However, this latter figure does not take into account the possibility of systematic error.

3.5. Modifications to Mass Spectrometer to Improve Precision

3.5.1. Thermal insulation of inlet

One source of experimental noise in the off-the-shelf instrument likely comes from temperature gradients. A temperature difference of several K can exist between the bellows, which are inside the mass spectrometer housing and warmed by heat from the pumps, and the sample volume, which is at room temperature. Because only 4/5 of the sample goes into the bellows and 1/5 remains behind in the stainless sample volume, the potential exists for thermal diffusion fractionation during the 3-min equilibration and expansion into the bellows. At 800 Pa, the diffusive relaxation time is ~40 s for this particular geometry, so 3 min is adequate for diffusive processes to exert

their influence. The sensitivity of δ^{40}Ar to thermal diffusion at room temperature is ~0.045‰/K in the mixture used (Grachev and Severinghaus, 1999), so the potential exists for artifacts of order 0.045/5 = 0.009‰/K in this setup.

To avoid thermal fractionation, we have thermally insulated the inlet from the rest of the mass spectrometer and cut away the panels on the front and side so that the inlet is in good contact with the room air. The stainless volume and the bellows are therefore nearly isothermal. We also reversed the orientation of the pumps so that their cooling fans blow warm air backward away from the inlet and installed a small fan under the inlet to further blow the warm air away. At the start of each run, we record the temperature of the two bellows to insure that the small difference (typically 0.6K) between them remains constant. We also wrap the bellows, capillaries, and changeover valves in insulating material to cut down on short-term temperature fluctuations. The room temperature is maintained constant to within ±0.5K, but most importantly, the rate of temperature change is generally <0.01K min^{-1}. This level of stability probably improves precision not only during equilibration, but also during the run because of temperature sensitivity of the amplifiers. The thermocouple that senses and controls the room temperature is attached to the amplifier housing to provide the amplifiers with maximum temperature stability. A strip chart records room temperature so anomalies can be noted.

3.5.2. Handling of standard can

Our working standard gases are kept in 10-cm diameter × 25.5-cm long cylindrical welded stainless steel cans with a volume of ~1800 cm^3. The can outlet, centered on the axis of the cylinder, has two stainless bellows valves (Nupro SS-4H-TW) welded together to form a 1.3-cm^3 pipette volume. Flow direction arrows on the valves both point away from the can. The valves are separated from the body of the can by 3 cm of 3/8″ OD stainless tubing. Gas pressure in the standard is ~3 × 10^4 Pa. To produce an aliquot, we evacuate the pipette, then expand the gas into the pipette and equilibrate for 3 min before expanding the aliquot into the mass spectrometer bellows. Temperature differences between the body of the can and the pipette can cause thermal fractionation at this step and are avoided.

Additionally, we maintain the can in a horizontal position, so that convection will not bring warm, thermally fractionated air to the outlet. We have observed fractionation during filling of vertically oriented flasks that were heated on one side (Severinghaus et al., 2001). We attribute this to a thin layer of rising warm air at the wall of the flask, which is bounded by a cooler sinking region in the flask interior, with thermal fractionation occurring horizontally across this temperature gradient. The result is a progressive depletion of the heavy isotope in the rising air, the phenomenon exploited in the Clusius-Dickel thermal diffusion column (Grew and Ibbs, 1952). Because the flasks are oriented with the exit port at the top, any fractionated warm air would preferentially leave the flask, causing a bias in the remaining air. Maintaining the flask in a horizontal orientation, with the outlet midway between the upper and lower walls of the flask, insures that warm fractionated air will not have a greater or lesser chance of exiting the flask than cool air.

3.5.3. Use of timers

We use timers so that each step is done for the same amount of time on each repeated measurement. Thus, any small leaks or time-dependent fractionation processes are to first order the same for both sample and La Jolla air (standard). These small fractionations will therefore cancel.

3.5.4. Ion gauge on inlet for leak detection

The off-the-shelf instrument comes with only a Pirani gauge on the inlet system, with limited sensitivity to pressures below 0.1 Pa. We installed a Bayert-Alpert-type ion gauge (Granville-Phillips) immediately in front of the inlet turbomolecular pump. This gauge is sensitive to 10^{-5} Pa and typically runs at 10^{-4} Pa. This allows detection of very small leaks in the inlet, which can affect the δ^{40}Ar because of fractionation occurring as gas passes through a small orifice.

3.5.5. Rapid opening of valves

Orifice fractionation as a valve is opened can be demonstrated to occur if a valve is opened very slowly. To minimize this type of fractionation, we attempt to open manual valves quickly.

3.5.6. Disconnected analog output cable

We run the mass spectrometer with the analog output cable disconnected from the electronics board. This several-m long cable could theoretically act as an antenna and pick up radio frequency signals that would add noise to the signal.

3.5.7. Minimize changeover valve delay

The software closes the mass spectrometer to one gas stream slightly before opening it to the other gas stream. The reason for this is to allow the dead volume in the valves to pump out and to reduce memory in the case of a "sticky" gas such as CO_2. For Ar, this is not necessary, so we minimize the delay. This reduces the pressure perturbation associated with switching and allows faster switching, which should lead to better precision. The delay time is an adjustable parameter in the System Tables in the ISODAT software.

3.5.8. Keeping pump oil out of the mass spectrometer

Hydrocarbons could theoretically interfere with Ar at mass 36. We minimize the amount of pump oil in the mass spectrometer by using oil traps (Lesker Micromaze) immediately in front of the rotary vane vacuum pumps. These are baked out periodically (every 6 months or so), during which time a valve (Lesker SA 0075MVQF) upstream of the traps is closed. We have found that it is not necessary to vent the mass spectrometer to bake the traps (the turbomolecular pumps can function with several hundred Pa of back pressure). Additionally, to avoid venting during power outages, which can result in oil getting into the mass spectrometer, we use an Uninterruptable Power Supply (UPS) (Mitsubishi 2033A).

Table 1. Example of the sequence of beam integrations for the δKr/Ar measurement.

#	Time (h:m:s)	Mass	Gas input	Resistor (Ohm)	Voltage	Integration Time (s)
1	9:23:08	84	Sample	1×10^{12}	0.279697	16
2	9:23:33	84	Standard	1×10^{12}	0.341211	16
3	9:24:54	36	Sample	3×11^{12}	1.969138	8
4	9:25:11*	36	Standard	3×10^{11}	1.972951	8
5	9:26:20	84	Sample	1×10^{12}	0.277693	16
6	9:26:45	84	Standard	1×10^{12}	0.338986	16
7	9:28:06*	36	Sample	3×10^{11}	1.955226	8
8	9:28:23	36	Standard	3×10^{11}	1.960496	8
9	9:29:34	84	Sample	1×10^{12}	0.275706	16
10	9:29:59	84	Standard	1×10^{12}	0.336868	16

* The times to which the voltages are interpolated, and the δ calculation is made.

3.5.9. Alteration of the interfering masses program

For improved precision during peak jumping, we made small modifications to the Interfering Masses program software. The off-the-shelf software forces the magnet to be reset between each measurement, even if it is the same mass, which takes ~30 s. Our modification allows the changeover valve to be operated without a magnet reset, so that standard and sample can be compared quickly for the same mass as is done in dual-collection mode. This saves time and increases precision, because instrument drift is minimized. The modification also produces six decimal places in the output voltages. These voltages and the times at which they were measured are written to an ASCII file automatically, simplifying the data analysis and permitting interpolation in time to correct for the falling pressures during the run.

3.6. Analysis of Krypton/Argon Ratio

The $^{84}Kr/^{36}Ar$ ratio is also measured in our ice core protocol. This ratio is useful as an indicator of argon loss, which may occur during bubble close-off or if the samples are warmed to near the melting point during core retrieval or handling (Bender et al., 1995). Krypton is a larger atom and is not as easily lost as argon, based on the observation that Kr/N_2 ratios are nearly unchanged in samples that have substantial Ar and O_2 loss (Severinghaus and Brook, 2000; see below). There is a possibility that argon loss may result in isotopic fractionation of the remaining gas, so care should be taken to prevent samples from warming above −10°C or so during shipping, storage, and handling. $^{84}Kr/^{36}Ar$ is also useful as an indicator of extensive snow melting and refreezing, as Kr is about twice as soluble in liquid water as Ar.

We measure Kr by peak jumping, after the $\delta^{40}Ar$ analysis is completed. Ten sequential integrations are made as shown in Table 1. The raw voltages are linearly interpolated to the times of the fourth and seventh measurements to correct for the effect of downward drift of the beams, and a δ value is calculated at the times of the fourth and seventh measurements:

$$\delta Kr/Ar \equiv [(V^{84}/V^{36}_{sample})/(V^{84}/V^{36}_{standard}) - 1]10^3‰ \quad (8)$$

These two values are averaged to give the result. For the example shown in Table 1, δKr/Ar = −179.20‰. Repeat runs of the same gas sample give a standard deviation of ~0.2‰, which can be considered an estimate of the internal precision. No pressure imbalance or chemical slope corrections are made, as these effects were shown to be negligible compared to internal precision (note, however, that this may not be true for other mass spectrometers or other tunings of the source parameters).

We normalize to the atmosphere in the same way as for $\delta^{40}Ar$, with the exception that no attempt is made to correct for drift of the standard over the course of a set of measurements due to the lower precision. La Jolla air values for δKr/Ar over the past 2 yr have a standard deviation of 0.67‰, but some of this is due to long-term drift in the standard (Fig. 6). During 2001, the values have a standard deviation of 0.31‰ ($n = 17$). Reproducibility of replicate ice samples cut from the same depth is worse; the pooled standard deviation of the GISP2 I8 set is 1.2‰. This suggests either that there is real variability in δKr/Ar from piece to adjacent piece in the ice samples or that our extraction technique imposes variable fractionations. Based on the observation that Ar/N_2 values also show similar scatter, the former seems more likely.

To assess the amount of gas loss from δKr/Ar, it is necessary to first correct for the effect of gravitational fractionation (Craig et al., 1988; Schwander, 1989; Sowers et al., 1989). This may be done by using the measured $\delta^{40}Ar$, if it is known that thermal diffusion is not an important fractionating mechanism (for example, if the ice is from a climatically stable period). Under these circumstances, gravity is the only process affecting $\delta^{40}Ar$. As the mass difference between ^{84}Kr and ^{36}Ar is 48 amu, $\delta^{84}Kr$ is 12 times as affected by gravity as $\delta^{40}Ar$. From this we obtain gravity-corrected $\delta^{84}Kr$:

$$\delta Kr/Ar_{gravcorr} \equiv \delta^{84}Kr - 12\ \delta^{40}Ar \quad (9)$$

The mean $\delta Kr/Ar_{gravcorr}$ for all Vostok samples is +5.0‰ ($n = 178$), and for the climatically stable parts of the GISP2 I1 and I8 sets, it is +5.6‰ ($n = 12$) and +6.0‰ ($n = 18$), respectively. Holocene GISP2 ice is generally +4 to 5‰. The figure for Siple Dome is +6.5‰ ($n = 175$). These figures suggest either that krypton is consistently enriched or argon is consistently depleted in polar ice by some factor other than gravity and thus suggest a complication to the use of $^{84}Kr/^{36}Ar$ as an indicator of gravitational fractionation and firn paleothickness as proposed by Craig and Wiens (1996).

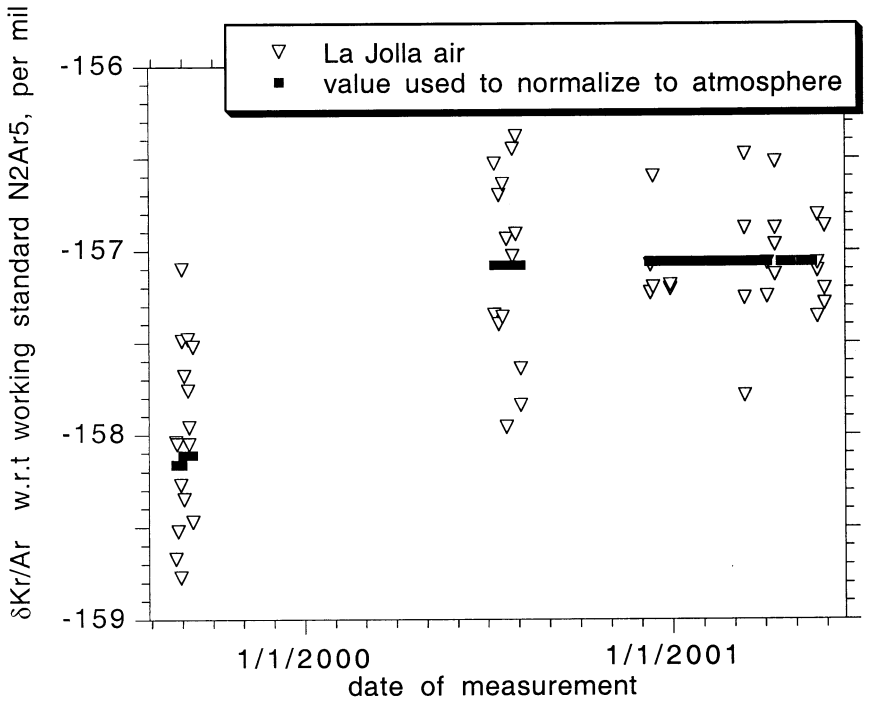

Fig. 6. Results of δKr/Ar measurements in the same La Jolla air samples as in Fig. 5.

4. PALEOENVIRONMENTAL APPLICATIONS

4.1. Greenland (GISP2) Abrupt Warming 15,000 Yr Ago

In Figure 7, we show (previously published) results of argon and nitrogen isotope measurements from the GISP2 ice core. In the following subsection, we will use these data to compute previously unpublished paleo-firn thicknesses. These data span the beginning of Interstadial 1 (the Oldest Dryas, Bølling Transition), when an abrupt warming took place (Severinghaus and Brook, 1999). The classical paleothermometer, the $\delta^{18}O$ of the ice, shows an abrupt increase from values of about −40‰ to values of about −36‰, starting at 14.7 kyr BP (before present, which is 1950 A.D.). This is the event that has been identified by numerous authors as the start of the Bølling warm interval or the Bølling Transition (Stuiver et al., 1995). Because of uncertainty in the classical $\delta^{18}O_{ice}$ paleothermometer (Cuffey et al., 1995), there is strong motivation to seek an independent estimate of the magnitude of the warming. The nitrogen and argon isotopes provide this as follows.

The observed nitrogen and argon heavy isotope enrichments may be expressed as the sum of two terms, the enrichment due to gravitational settling $\delta^{15}N_{grav}$ and that due to thermal diffusion $\delta^{15}N_{therm}$:

$$\delta^{15}N_{observed} = \delta^{15}N_{grav} + \delta^{15}N_{therm} = \delta^{15}N_{grav} + \Omega^{15}\Delta T \quad (10)$$

$$\delta^{40}Ar_{observed} = \delta^{40}Ar_{grav} + \delta^{40}Ar_{therm} = \delta^{40}Ar_{grav} + \Omega^{40}\Delta T \quad (11)$$

where Ω^{40} and Ω^{15} are the thermal diffusion sensitivities of the argon and nitrogen isotope pairs, respectively, and ΔT is the temperature difference between the top and bottom of the firn, which is nearly equal to the magnitude of the abrupt warming in the few decades following an abrupt warming (a heat transfer model of the firn treats this relationship explicitly; see Severinghaus et al., 1998). The Ω values are determined from laboratory measurements (Grachev and Severinghaus, 2003). We take advantage of the fact that gravitational settling increases as the mass difference Δm (which is 4 for $\delta^{40}Ar$ but only 1 for $\delta^{15}N$) such that $\delta^{15}N_{grav} = \delta^{40}Ar_{grav}/4$ (Craig et al., 1988). Dividing Eqn. 11 by 4 and subtracting it from Eqn. 10, the gravitational terms cancel, and we have

$$[\delta^{15}N - \delta^{40}Ar/4] = \Delta T(\Omega^{15} - \Omega^{40}/4) \cong \Delta T(0.0143‰\ K^{-1} - 0.0097‰\ K^{-1}) \quad (12)$$

The difference $[\delta^{15}N - \delta^{40}Ar/4]$ is defined as a new parameter, $\delta^{15}N_{excess}$, which is thus a proxy for paleo-firn temperature gradient with sensitivity $\cong +0.0046‰\ K^{-1}$ (at a mean temperature of 230K; the sensitivity changes slightly with the mean temperature; Severinghaus et al., 2001).

$$\delta^{15}N_{excess} \equiv [\delta^{15}N - \delta^{40}Ar/4] = \Delta T\ 0.0046‰\ K^{-1} \quad (13)$$

The pooled standard deviation of the Bølling data set is 0.010‰ for $\delta^{15}N$ and 0.005‰ for $\delta^{40}Ar/4$, thus suggesting for this data set a precision of $(0.010^2 + 0.005^2)^{0.5}/0.0046 = \pm 2.4K$. Figure 8 shows calculated $\delta^{15}N_{excess}$ across the Bølling Transition, with model predictions for various magnitudes of "step function" warmings. The model is a heat and gas diffusion model of the firn that is described in detail elsewhere (Severinghaus and Brook, 1999; Severinghaus et al., 2001). A

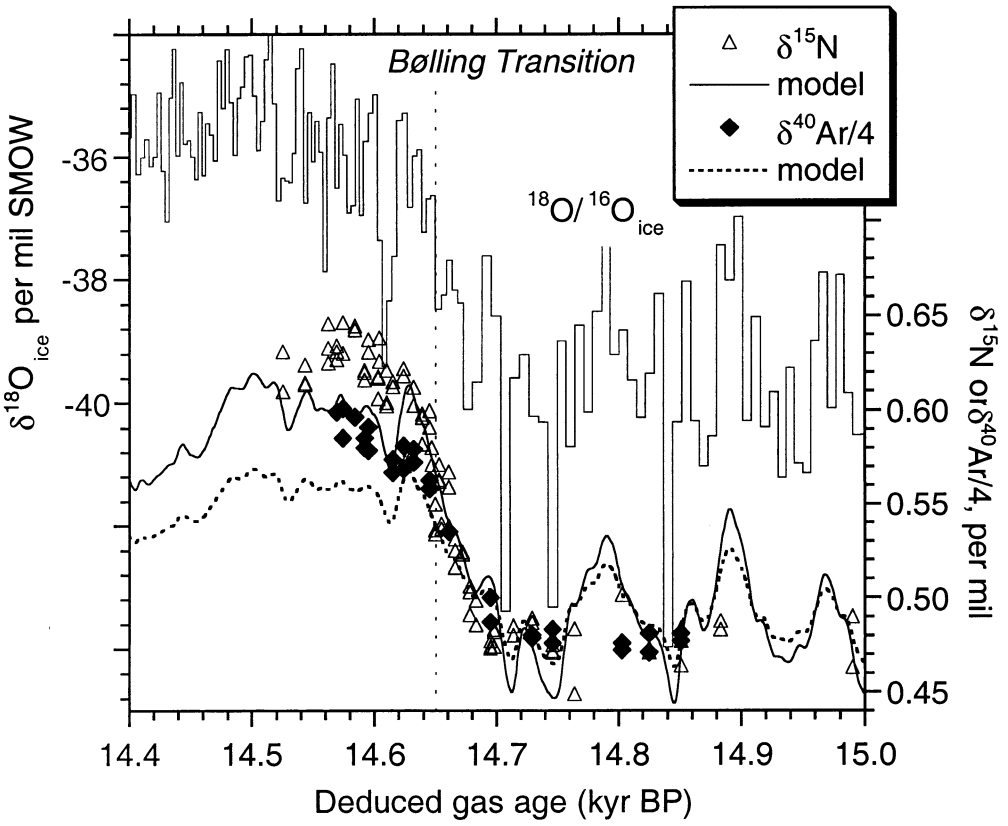

Fig. 7. An example of argon and nitrogen isotope data from the end of the last glacial period at the Bølling Transition in the GISP2 ice core (adapted from Severinghaus and Brook, 1999). The classical method of temperature reconstruction is by the oxygen isotope ratio of the ice, shown at the top (Stuiver et al., 1995). The model curves were produced by assuming that the ^{18}O record gives the temperature correctly when calibrated by the borehole temperature method (Cuffey et al., 1995), then driving a forward model of heat and gas diffusion in the firn that incorporates gravitational settling and thermal diffusion (Severinghaus and Brook, 1999). No attempt was made to include changes in gravitational settling in the model, yet ~6 m of firn deepening is likely to have occurred (see text), which may explain the mismatch of the model and data in the age range 14.55 to 14.6 kyr BP. Argon data are divided by 4 for direct comparison with nitrogen. The difference between argon and nitrogen isotopes reflects thermal diffusion, because argon isotopes are less sensitive to thermal diffusion than nitrogen isotopes on a per mass unit basis. The gas age was deduced by minimizing the mismatch of the model and data and is thus independent of glaciologic estimates of the gas age-ice age difference (see Severinghaus and Brook, 1999).

step function warming of roughly 11 ± 3K appears to best fit the data (Fig. 8). This value differs from the 9 ± 3 reported by Severinghaus and Brook (1999) because of recent improvements in the estimate of thermal diffusion sensitivity (Severinghaus et al., 2001; Grachev and Severinghaus, 2003).

4.2. Greenland (GISP2) Firn Thickness 15,000 Yr Ago

The paleo-thickness of the diffusive column (also known as diffusive column height or DCH) is calculated by first extracting the gravitational component of the observed fractionation. The effects of thermal diffusion are removed by solving Eqn. 10 and 11 for $\delta^{40}Ar_{grav}$ and employing observed $\delta^{15}N$ as follows (Severinghaus and Brook, 1999; Severinghaus et al., 2001):

$$\delta^{40}Ar_{grav} = 4[\delta^{40}Ar - \delta^{15}N(\Omega^{40}/\Omega^{15})]/[4 - \Omega^{40}/\Omega^{15}] \quad (14)$$

Then the DCH is calculated from the barometric equation (Sowers et al., 1992), where R is the gas constant = 8.314 J K^{-1} mol^{-1} and Δm is the mass difference between ^{40}Ar and ^{36}Ar = 0.00400 kg mol^{-1}:

$$DCH = RT \ln[(\delta^{40}Ar_{grav})10^{-3} + 1]/(\Delta mg) \quad (15)$$

For calculating DCH here, we used $\Omega^{40}/\Omega^{15} = 2.60 \pm 0.08$ (1 standard deviation), the value obtained from firn air experiments at Siple Dome and South Pole (Severinghaus et al., 2001), and T = 226K (strictly speaking T should vary with time, but the effect of temperature is second-order). The resulting DCH is shown in Figure 8. A slight deepening of the column may be evident, from a mean 92 m before the Transition to a mean 97 m afterward, although this difference is probably not significant given that the analytical uncertainty is large. If T were allowed to vary (using the warming of 11K obtained above), this deepening would be more pronounced by ~2 m. For comparison, a ~6-m transient deepening is expected from glaciologic modeling of the firn due to the large increase in snow accumulation rate at this event (Schwander et al., 1997).

During times of constant or very slowly changing climate

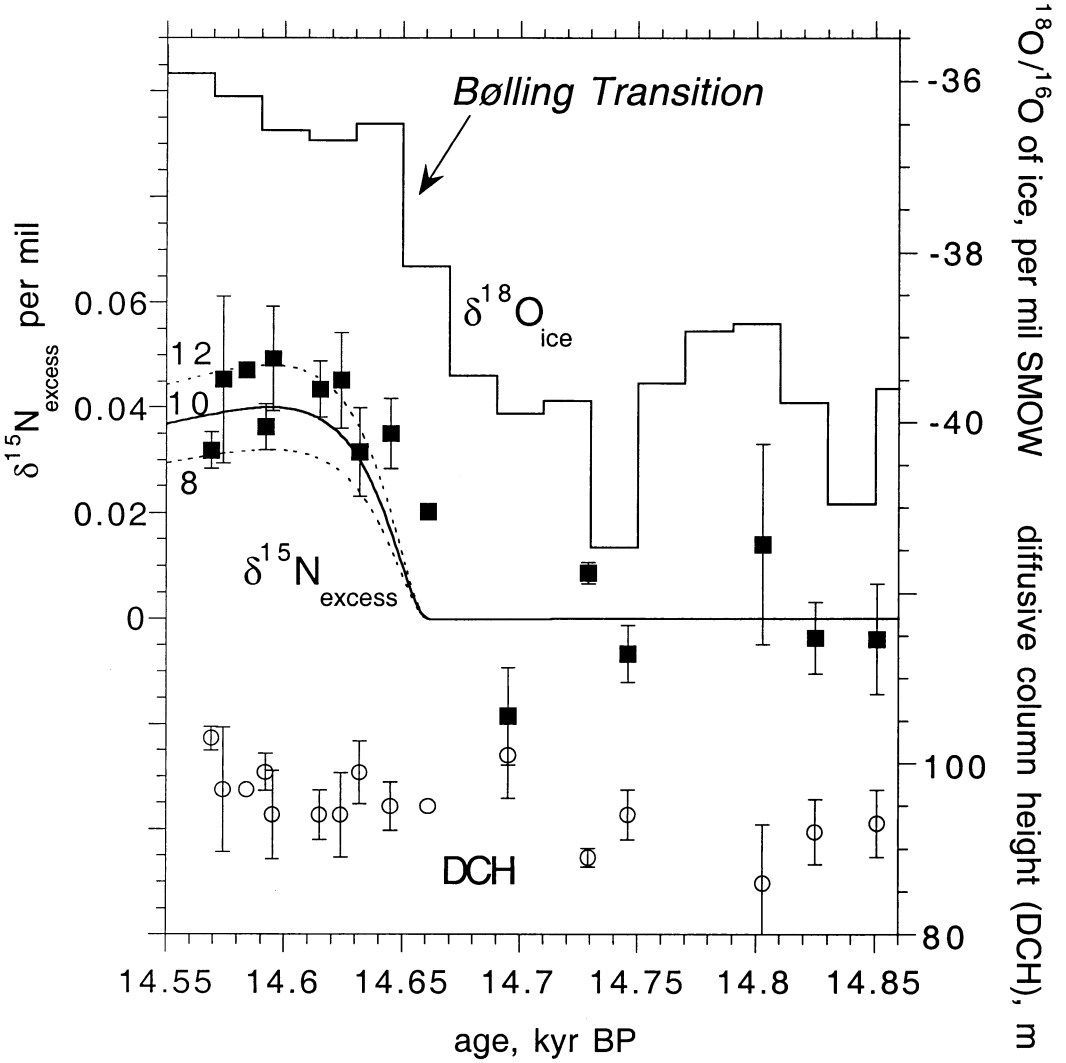

Fig. 8. Derived parameters $\delta^{15}N_{excess} \equiv \delta^{15}N - \delta^{40}Ar/4$ (which is insensitive to gravitational settling) and DCH at the Bølling Transition. The error bars reflect the standard deviations of the two ($\delta^{40}Ar$) or 3 ($\delta^{15}N$) replicate ice samples from each depth, with error propagation assuming the errors are uncorrelated. The $\delta^{15}N_{excess}$ values are compared with the model predictions for step-function increases in temperature, suggesting a warming of 11 ± 3K at the transition. No model error estimate is shown, but it is likely <3%, and so it is dwarfed by the analytical uncertainty.

(<0.01K yr^{-1}), it may be assumed that thermal diffusion is negligible, and under these conditions, it is not necessary to measure $\delta^{15}N$, and DCH may be estimated from $\delta^{40}Ar$ alone.

The presence of a wind-mixed "convective zone" near the surface (Colbeck, 1989; Sowers et al., 1992) may cause the DCH to be less than the total firn thickness, if mixing in this layer is vigorous enough to dominate molecular diffusion as a vertical transport mechanism (Craig et al., 1988). However, no conclusive evidence exists for such domination at Siple Dome or the South Pole today (Battle et al., 1996; Severinghaus et al., 2001), although it has been reported at Vostok (Bender et al., 1994b). It should be noted that the existence of convective air motions does not by itself imply that isotope fractionation cannot proceed, because molecular diffusivity of gases in near-surface firn is rather fast (~1 m^2 day^{-1}; Schwander et al., 1988). Only if the effective vertical eddy diffusivity due to convection exceeds this amount will isotope fractionation be thwarted. Nonetheless, uncertainty about possible changes in past thickness of the convective zone (due to greater wind speed, surface roughness, or snow permeability, for example) requires that we consider the DCH to be only a minimum estimate of firn thickness. Also, firn thickness may be greater than DCH because of a 5- to 10-m thick "non-diffusive zone" (Sowers et al., 1992) near the firn-ice transition. Such a zone may originate from horizontal impermeable layers that cut off the gases from further gravitational fractionation despite bulk densities that are lower than the expected value for the firn-ice transition (Martinerie et al., 1992).

Despite these limitations, the DCH estimates presented here agree well with calculated firn thickness from a glaciologic model (Herron and Langway, 1980), using as inputs the reconstructed temperature and accumulation rate from borehole ther-

mometry and annual layer counting (Cuffey and Clow, 1997). Assuming a temperature of 226K and an accumulation rate of 0.075-m ice yr^{-1} during the cold period of constant climate preceding the Bølling Transition, the Herron-Langway model predicts a firn thickness of 95 m, close to our mean DCH value of 92 m. This calculation uses the close-off density of Martinerie et al. (1992) as modified for GISP2 by Schwander et al. (1997). However, gas-loss-induced fractionation may bias our estimate upward by ~6 m (see below).

4.3. Greenland (GISP2) Krypton/Argon Ratios 15000 Yr Ago

To evaluate gas loss from δKr/Ar in ice that formed during periods of rapid climatic change, it is necessary to correct for both gravitational and thermal diffusion effects. This is done by using the argon and nitrogen isotope data to isolate the gravitational and thermal components and then subtracting appropriately scaled terms for the gravitational and thermal effects on δKr/Ar. This yields a parameter called "$\delta Kr/Ar_{gravthermcorr}$" that is corrected for gravitational and thermal effects:

$$\delta Kr/Ar_{gravthermcorr} \equiv \delta Kr/Ar - 48\ \delta^{15}N_{grav} - \Omega^{84}/\Omega^{15}\ \delta^{15}N_{therm} \quad (16)$$

The factor of 48 arises because the mass difference of the ^{84}Kr - ^{36}Ar pair is 48 compared to one for ^{15}N - ^{14}N. The ratio of thermal diffusion sensitivities Ω^{84}/Ω^{15} is 16.3 (Severinghaus et al., 2001). An analogous parameter is calculated for the measured $^{40}Ar/N_2$ ratio (measured on separate pieces of ice by the technique of Sowers et al., 1989):

$$\delta^{40}Ar/N_{2gravthermcorr} \equiv \delta^{40}Ar/N_2 - 12\ \delta^{15}N_{grav} - \Omega^{Ar/N2}/\Omega^{15}\ \delta^{15}N_{therm} \quad (17)$$

The ratio of the thermal diffusion sensitivities is ~16 (Grew and Ibbs, 1952). For the purpose of comparison with δKr/Ar, the inverted ratio $\delta N_2/^{40}Ar$ is calculated as:

$$\delta N_2/^{40}Ar_{gravthermcorr} = [1/(\delta^{40}Ar/N_{2gravthermcorr}10^{-3} + 1) - 1]\ 10^3‰ \quad (18)$$

The measured δKr/Ar for the Bølling data set is shown in Figure 9, along with $\delta^{40}Ar$ for reference. Note that the values are rather constant across the transition at about +30‰. This reflects the relatively weak thermal diffusion sensitivity of δKr/Ar compared to its gravitational sensitivity. The corrected parameter $\delta Kr/Ar_{gravthermcorr}$, shown at the bottom of Figure 9, is even more constant across the transition, with an average of +5.0‰ and +5.4‰ before and after the climate transition, respectively. This constancy provides a (rough) consistency check on the thermal diffusion sensitivities used here, as errors in these values would lead to non-constant values across the transition. Interestingly, the $\delta N_2/^{40}Ar_{gravthermcorr}$ (shown as circles in Fig. 9) is very similar to $\delta Kr/Ar_{gravthermcorr}$, suggesting that the common reason that both parameters are not zero is due to loss of argon rather than anomalous enrichment of the other gases. Such loss of argon probably occurs during the bubble close-off process, as suggested by observations of elevated argon concentration in basal firn air (Severinghaus and Brook, 2000). Atmospheric changes in these ratios due to solubility effects in the colder ocean are probably <~2‰ and so may be neglected (Craig and Wiens, 1996).

4.4. Argon Isotope and Kr/Ar Data from Siple Dome, West Antarctica

Siple Dome is a coastal ice dome on the eastern margin of the Ross Ice Shelf, where a 1004-m ice core to bedrock was retrieved between 1997 and 1999. The last glacial termination occurs at ~600- to 700-m depth. We present here a high-resolution $\delta^{40}Ar$ and δKr/Ar data set that reveals two climatic events during the deglaciation. These data span the 665- to 740-m depth interval, which corresponds approximately to the 22,000- to 12,000-yr BP time interval.

We caution the reader that a small isotopic fractionation may accompany argon loss, either during bubble closure or during core retrieval and handling. Work in progress (to be published separately) points to an enrichment of $\delta^{40}Ar$ of +0.007‰ per ‰ enrichment of δKr/Ar in the Siple Dome data set. We have attempted to correct the data set from the Siple Dome ice core for this effect using the measured $\delta Kr/Ar_{gravcorr}$ as a proxy for argon loss. In this first attempt, we neglect the effect of thermal diffusion on δKr/Ar, as the magnitude of the thermal diffusion effect on δKr/Ar is only 0.24‰ K^{-1} (Severinghaus et al., 2001). We adopt a value of +0.007‰ per ‰ as an empirical gas-loss correction factor:

$$\delta^{40}Ar_{gaslosscorr} = \delta^{40}Ar - 0.007\ \delta Kr/Ar_{gravcorr} \quad (19)$$

where

$$\delta Kr/Ar_{gravcorr} = \delta Kr/Ar - 12\ \delta^{40}Ar_{gaslosscorr} \quad (20)$$

Eqn. 19 and 20 are solved for $\delta^{40}Ar_{gaslosscorr}$

giving

$$\delta^{40}Ar_{gaslosscorr} = [\delta^{40}Ar - 0.007\ \delta Kr/Ar]/(1 - 0.007 \times 12) \quad (21)$$

As the typical $\delta Kr/Ar_{gravcorr}$ in ice cores is about +6‰, the correction will typically be about −0.045‰. This corresponds to −2 m in the reconstructed firn depth during periods of constant climate, or roughly −6 m during periods of climatic change when $\delta^{15}N$ is used to separate gravitational effects from thermal diffusion effects. In this situation, δKr/Ar is also affected by thermal diffusion, so strictly speaking, three simultaneous equations with three unknowns should be solved, which we leave for future work. However, we note that $\delta Kr/Ar_{gravthermcorr}$ is fairly constant at ~6‰ across the very large temperature change at the GISP2 Bølling Transition (Fig. 9), suggesting that gas loss was fairly constant across this event. Correction of this data set for gas loss-induced fractionation would therefore increase $\delta^{15}N_{excess}$ by 0.045/4 = 0.011‰ both before and after the climate event but would have no substantial effect on the inferred amplitude of the climate warming, which depends on the difference between $\delta^{15}N_{excess}$ values before and after. It would, however, reduce the inferred DCH by ~6 m. This would widen the discrepancy with the glaciologic estimate of firn thickness to 9 m.

The corrected Siple Dome results are presented along with the uncorrected data in Figure 10. Two features of the record

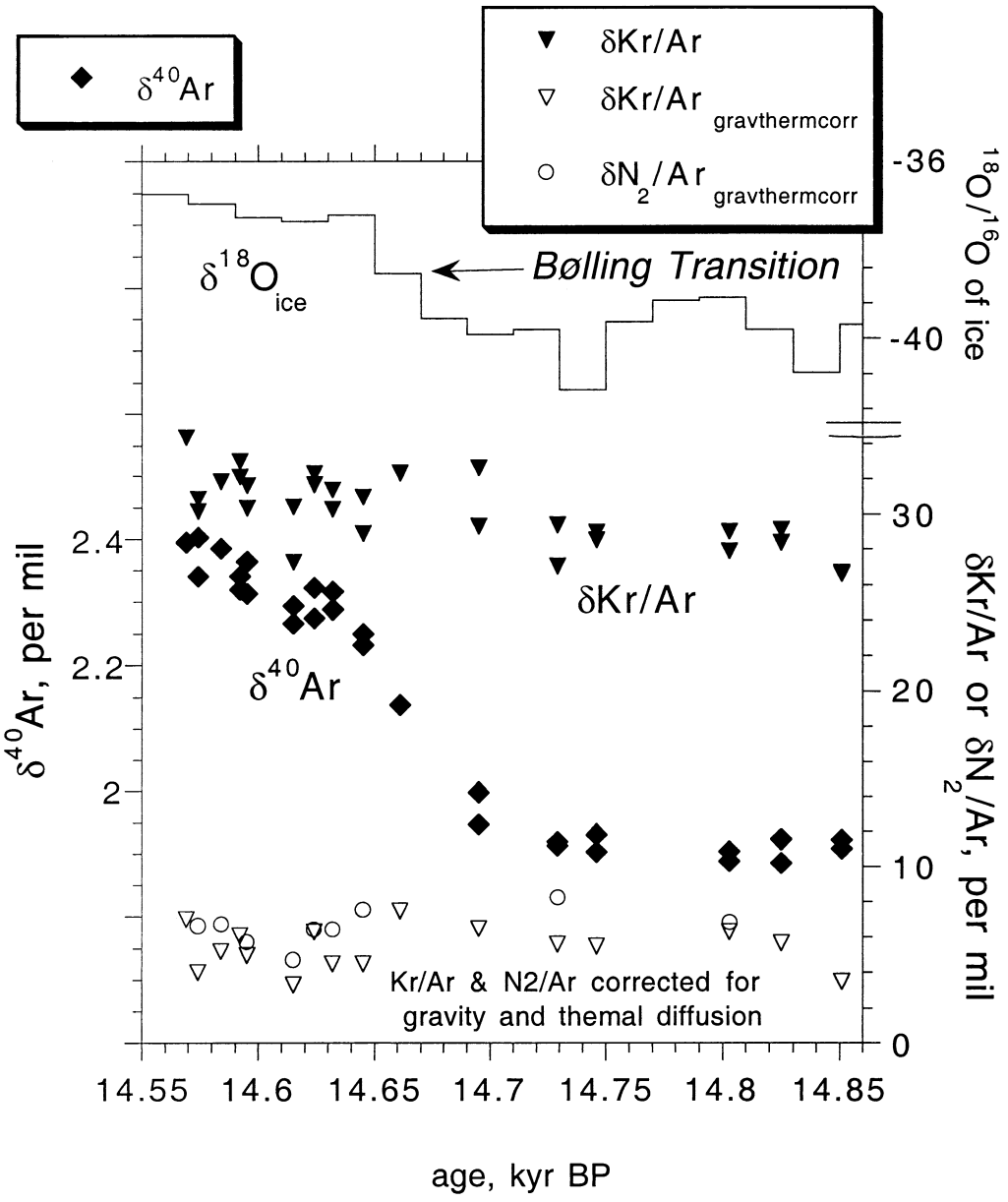

Fig. 9. Measured δKr/Ar at the Bølling Transition, with argon isotope and N_2/Ar ratios shown for comparison. The open symbols have been corrected for gravitational and thermal diffusion effects, so they should be zero if gravity and thermal diffusion were the only processes affecting them. The consistently positive values of about +5‰ agree with measurements from other ice cores (see text) and suggest that argon generally is fractionated relative to nitrogen and krypton in polar ice, probably due to the bubble close-off process.

are noteworthy. At 727 m, δ^{40}Ar steps down by ~0.36‰, 5-m deeper in the core than an abrupt increase in H_2O isotopes that has been interpreted as an abrupt warming event (James White, pers. comm.). This depth in the core corresponds to sometime between 18 and 22 kyr BP on the preliminary methane-based time scale (Edward Brook, pers. comm.). The step-like decrease in δ^{40}Ar is accompanied by a nearly identical decrease in δ^{15}N (data not shown), suggesting that the change is primarily due to gravitational settling. Assuming an average temperature of 235K, the decrease would correspond to an 18-m reduction of DCH. Assuming no change in convective zone thickness, this implies an 18-m reduction in firn thickness. If the water isotopes (δ^{18}O and deuterium of ice) may be interpreted classically as a proxy for temperature, then the thinning of the firn would be the expected result of a ~20 to 50% decrease in accumulation rate using the Herron and Langway (1980) firn densification model. The 5-m offset of the ice and gas signals is an expected consequence of the gas age-ice age difference (Schwander et al., 1993), which arises from the fact that the bubbles are closed off at the base of the firn layer.

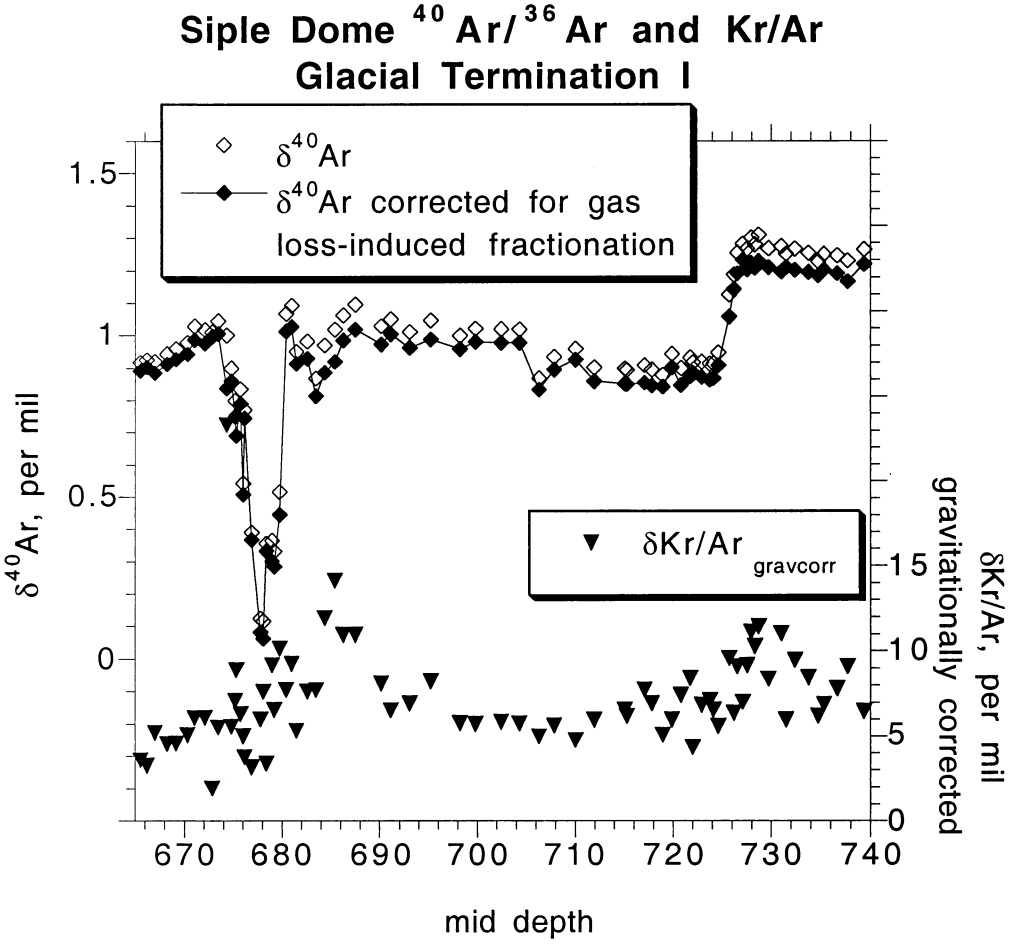

Fig. 10. Argon isotope and δKr/Ar data from Siple Dome ice core, West Antarctica, 665- to 740-m depth. This interval spans the time interval from ~12 to 22 kyr BP. The $\delta Kr/Ar_{gravcorr}$ was calculated using Eqn. 20 and thus takes into account the correction for gas loss.

Thinning by compaction and ice flow has presumably reduced the original ~60-m thickness of firn to 5 m. This 5-m offset provides critical evidence that the abrupt shift in water isotopes is not an artifact due to a tectonic dislocation or a hiatus in deposition. In these cases, the gas and ice signals would be expected to occur at the same depth.

A second feature at 678 m commands attention with a unique drop of $\delta^{40}Ar$ to nearly zero, a value never seen before in polar ice (Fig. 10). The age of this event is 15.3 kyr BP on the preliminary methane-based time scale (Edward Brook, pers. comm.). Again, $\delta^{15}N$ shows very similar patterns, suggesting that gravitational fractionation went essentially to zero at the bubble close-off horizon at that time. Beginning at 676.8 m, the gravitational signal appears to recover quickly, suggesting that the diffusive column was restored to its normal thickness in just a few centuries. A complex series of changes in water isotopes occurs at this time but defy simple explanation (James White, pers. comm.). The borehole optical log (Bay et al., 2001) shows a light-scattering and light-absorbing feature at 675- to 680-m depth, which may be an interval of elevated dust concentration. Two hypotheses have been proposed for this event: (1) An interval of sustained net ablation may have removed nearly all of the firn, so that the DCH was zero long enough for gases to be trapped that bear no gravitational signal. This situation corresponds to the "blue ice" zones of net ablation common near the Transantarctic Mountains today. (2) Alternatively, a small amount of ablation may have removed the top few meters of the firn, which exhibit low permeability at Siple Dome today (Albert et al., 2000) and may have served to isolate the firn from windpumping and other convective processes (Colbeck, 1989; Sowers et al., 1992). This removal may have allowed convective mixing of the entire firn column, reducing the DCH to zero. No modern analog of hypothesis (2) has been demonstrated to exist to our knowledge, but theoretical considerations of the effect of grain size on the permeability of firn to air flow suggest that this hypothesis is possible (Richard Alley, pers. comm.). Hypothesis (2) has the advantage that it can explain the abrupt 50% drop in $\delta^{15}N$ and $\delta^{40}Ar$ at 680 m over just ~30 cm of core (corresponding to ~40 yr) (Fig. 11). This is because removal of a few meters of firn could happen in a few years, whereas removal of the entire firn is expected to take many centuries.

A detailed view of the "678-m event" (Fig. 11) shows that $\delta^{40}Ar$ values consistently exceed $\delta^{15}N$ values during the low-$\delta^{40}Ar$ interval, leading to negative $\delta^{15}N_{excess}$ values. These

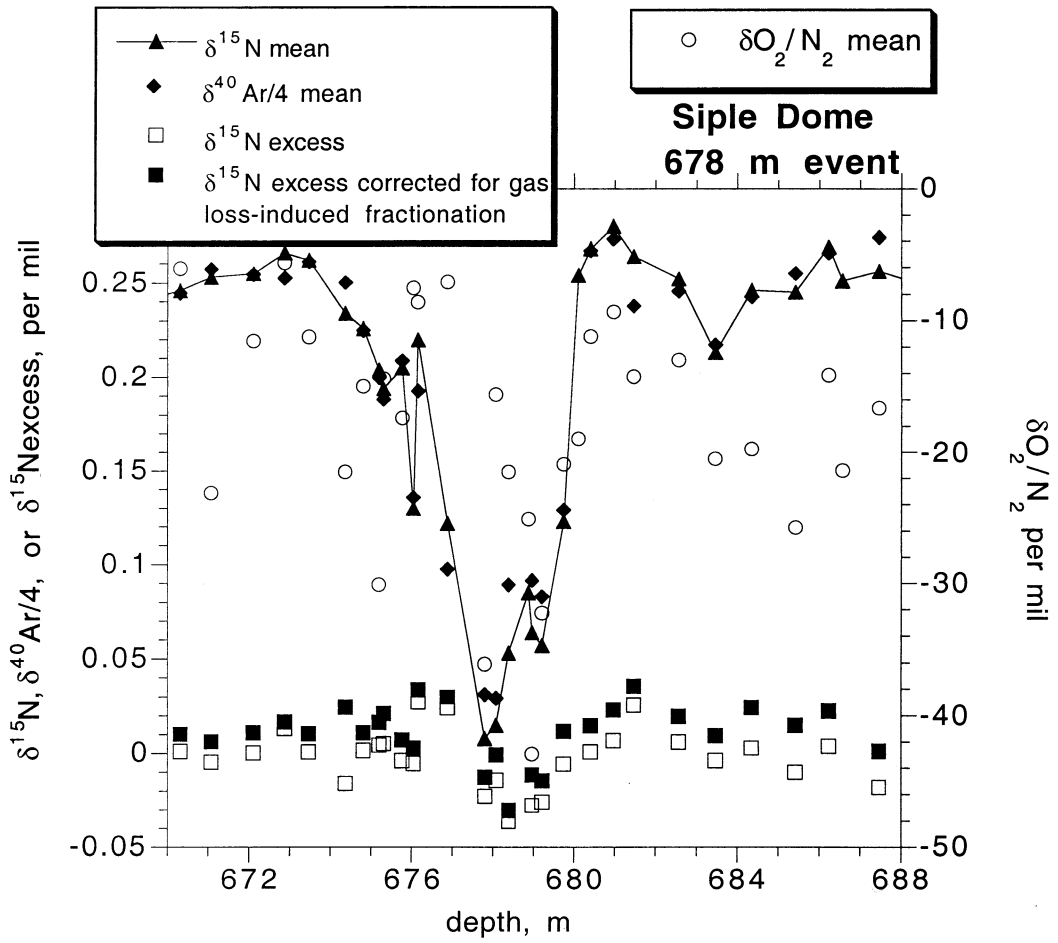

Fig. 11. Mean $^{40}Ar/^{36}Ar$, $^{15}N/^{14}N$, and O_2/N_2 data from the "678 m event," spanning the approximate time window of ~14 to 16.5 kyr BP. $\delta^{15}N_{excess}$ is shown to emphasize the negative (physically unrealistic) values in the depth interval with low $^{15}N/^{14}N$ values, which imply little or no DCH.

values go as low as −0.035‰. If the $\delta^{15}N_{excess}$ is interpreted strictly as a temperature signal, using Eqn. 13, this would imply that the top of the diffusive column was 7K colder than the bottom of the diffusive column. However, the thickness of the diffusive column here is nearly zero. Temperature equilibrates in less than a year over a thickness of a few meters in polar firn (Paterson, 1969), and yet the gradual bubble close-off process requires persistence of a temperature gradient for many decades for an isotopic signal of thermal diffusion to be recorded. Thus, it is extremely unlikely that these negative $\delta^{15}N_{excess}$ values reflect temperature gradients. This forces us to accept that there must be other processes besides thermal diffusion and gravitational settling causing isotope fractionation here. The low O_2/N_2 values during this anomalous interval (Fig. 11) point to gas loss as a possible third fractionation process, as O_2/N_2 is highly depleted in samples that have undergone gas loss (Bender et al., 1995). However, even our attempted correction for gas loss falls short of bringing $\delta^{15}N_{excess}$ to the expected value of zero in this extremely thin diffusive column (Fig. 11). Thus, there must be either a greater gas-loss fractionation than estimated or a fourth process has fractionated gases at this particular location in the core.

Importantly, no fractionation process is known to deplete ^{40}Ar in the retained gas. Therefore, those cases where $\delta^{40}Ar$ is less than $\delta^{15}N$, corresponding to positive $\delta^{15}N_{excess}$, are unlikely to be artifacts and probably do in fact represent warming episodes. Two such points at 676.9 and 676.2 m may indicate a rapid warming, coinciding with the recovery of the diffusive column at the end of the "678 m event" (Fig. 11). Interestingly, these points have high O_2/N_2 values (Fig. 11), which is consistent with little or no gas loss. This raises the speculation that gas loss may be a function of accumulation rate, with the rapid accumulation (inferred from the recovery of the DCH) preventing the gas loss.

Also, $\delta^{15}N_{excess}$ exhibits a step-like increase coincident with the "727 m event" that probably reflects a real warming event (Fig. 12). The mean of 11 points before 727 m is significantly ($P < 0.001$) different from the mean of the 11 points following 727 m (uncorrected values). The correction for gas-loss fractionation appears not to erase the step, and, therefore, it seems unlikely that it is an artifact (Fig. 12). The slight lag of the thinning of the diffusive column behind the step increase in $\delta^{15}N_{excess}$ is expected, due to the century-scale time required for heat to diffuse to the firn-ice transition and accelerate the

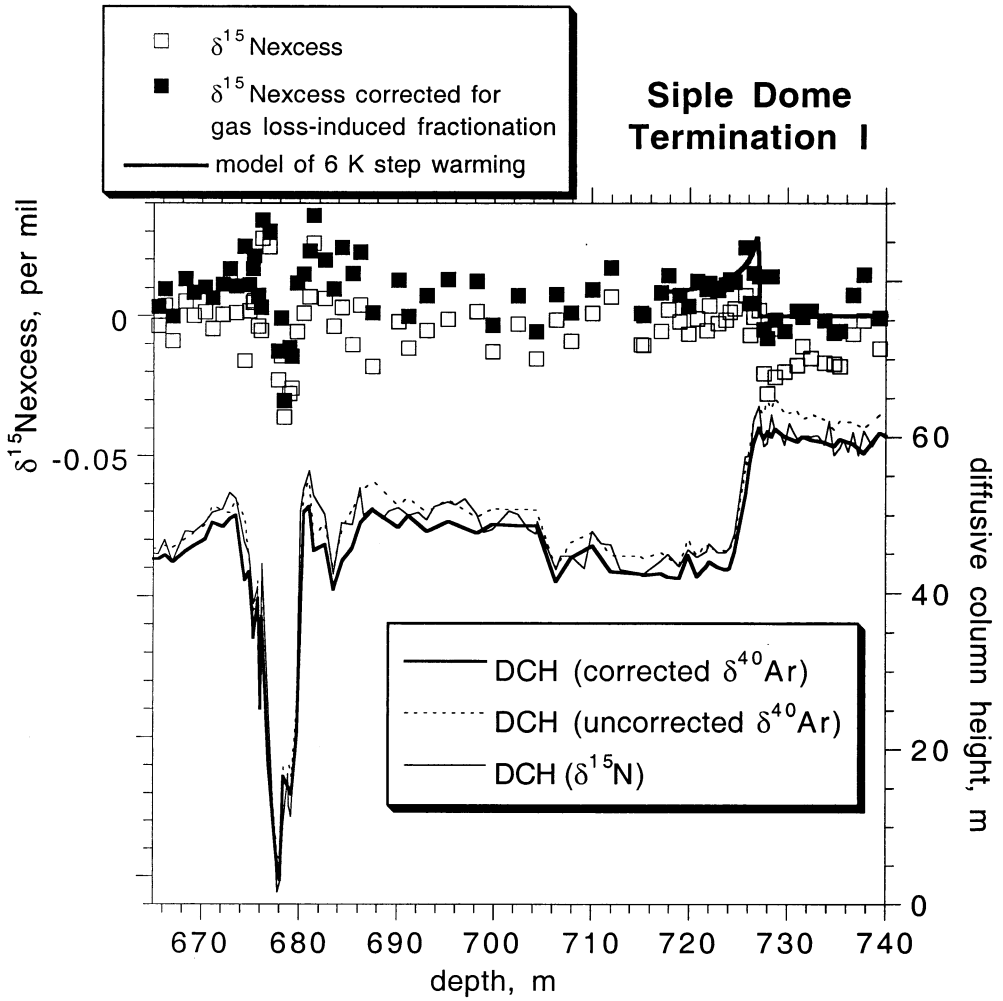

Fig. 12. Derived parameters $\delta^{15}N_{excess}$ and DCH in the Siple Dome ice core, 665- to 740-m depth. DCH values are shown for three different cases (see text). All cases assume that gravitational settling is the only fractionating process. For the interval immediately following the 727-m warming event, where thermal diffusion likely adds to the signal, this assumption probably results in values that are several meters too thick. A model prediction of $\delta^{15}N_{excess}$ for a 6K step-function warming is shown (constant temperature before and after the event with an instantaneous warming).

densification process leading to thinner firn. Calculated DCH is shown (Fig. 12) for three different cases: (1) based on corrected δ^{40}Ar, (2) based on uncorrected δ^{40}Ar, and (3) based on δ^{15}N. For this calculation we neglected thermal diffusion (assuming $\delta^{40}Ar = \delta^{40}Ar_{grav}$ and using Eqn. 15) and assumed a constant temperature of 235K and a gravitational acceleration of 9.82-m s^{-2}. We suggest that the corrected δ^{40}Ar gives the most accurate estimate of DCH, except in the middle of the 678-m event, where the δ^{15}N-based estimate is probably more accurate in light of the preceding discussion on gas loss.

5. SUMMARY

We present a high-precision method for measuring the argon-40 to argon-36 ratio in samples of glacial ice containing trapped air. The overall precision obtained for duplicate analyses of an ice sample (~100 g) is ~0.012‰ (1 standard error of the mean). For reconstructions of firn depth at times in the past in an ice core record, based on gravitational fractionation in the diffusive part of the firn column, this corresponds to a precision of ±0.6 m. Systematic error is probably larger but is difficult to quantify. For reconstructions of abrupt warming, precision is about ±2K, its exact value depending on the precision of the δ^{15}N measurements.

Sample size is ~45 g of ice, which yields ~0.04 standard cm^3 of argon by a wet extraction and gettering technique. To reduce the use of precious ice core sample, we dilute the extracted gas by a factor of 10 with tank N_2 before mass spectrometry. A 35-min analysis comprising 48 separate cycles of 8-s integrations yields an internal precision of about ±0.010‰. Mass spectrometric results must be corrected for imbalance in pressure (or ion current) between sample and standard and for differences in the N_2/Ar ratio between sample and standard. Normalization of the results to atmosphere, our ultimate reference gas, is done by measuring samples of air from outside the laboratory building (La Jolla air) against the same working standard gas used for the ice samples. Precision

is increased by controlling the thermal environment of the inlet and handling the standard can so as to avoid thermal fractionation, among other precautions.

Krypton/argon ratios are also measured, after the isotope ratio analysis, by peak jumping for two cycles of 16-s integrations. Air samples measured in duplicate give an overall precision of about ±0.22‰ (1 standard error of the mean). The figure for ice core samples measured in duplicate is about ±1‰, probably because of real variability from ice sample to adjacent ice sample in the core. Krypton/argon ratios can provide information about argon loss during bubble close-off or sample storage and handling, which may cause artifactual fractionation of the 40/36 ratio. Samples for argon isotope analysis should be stored at −10°C or colder to avoid argon loss. After correcting for gravitational effects, krypton/argon is generally ~5‰ enriched in ice core samples, probably due to loss of argon by size-dependent preferential exclusion of the smaller argon atoms during bubble close-off.

Application of these new tracers to paleoenvironmental studies shows that central Greenland warmed abruptly at the end of the last glacial period, and the magnitude of the warming was equivalent to an 11 ± 3K step-function increase. This result confirms the reality of the temperature shifts already inferred from oxygen isotopes of the ice. It further shows that their magnitude was larger than would be inferred from the classical application of the oxygen isotope "thermometer" but similar to the result obtained from borehole thermometry (Cuffey et al., 1995). Calculated DCH across this event agrees within error with independent estimates based on glaciologic models.

Results from the Siple Dome core (from West Antarctica) show two rapid climatic events during Termination I. First, an abrupt warming occurred at sometime between 18 and 22 kyr BP accompanied by a reduction in firn DCH from 61 to 43 m, which was probably due to a decrease in accumulation rate. This contrasts with Greenland, where accumulation always increases with abrupt warming (Alley et al., 1993). Second, an interval of ablation and removal of part or all of the firn appears to have occurred at 15.3 kyr BP. This may be related to a low- or no-accumulation event of similar age at Taylor Dome, located on the other side of the Ross Sea. This event raises the possibility that the ice record from Siple Dome has a short hiatus in this interval.

Acknowledgments—Michael Bender provided key ideas, mentoring, and laboratory facilities. Todd Sowers pioneered the extraction technique. Joe Orchardo taught one of us (J.P.S.) critical gas-handling and mass spectrometer maintenance techniques. Ralph Keeling suggested many of the improvements to increase precision and generously shared equipment. Derek Mastroianni made the GISP2 I8 and Siple Dome measurements. Margaret Ricci of Pennsylvania State University made the modifications to the ISODAT software for the Interfering Masses program. Reviews by Andrew Dickson, Heiri Baur, Martin Stute, and one anonymous reviewer improved the manuscript. The National Ice Core Laboratory in Denver, Colorado provided ice samples and assistance in cutting and shipping. J.P.S. was supported by a NOAA Climate and Global Change Postdoctoral Fellowship from 1995 to 1997 in the Bender laboratory at the University of Rhode Island, where much of the development work was done. This work was supported by NSF awards ATM99-05241 and OPP97-25305 (to J.P.S.).

Associate editor: R. Wieler

REFERENCES

Albert M. R., Shultz E. F., and Perron F. E. (2000) Snow and Firn Permeability at Siple Dome, Antarctica. *Ann. Glaciol.* **31,** 353–356.

Alley R. B., Meese D. A., Shuman C. A., Gow A. J., Taylor K. C., Grootes P. M., White J. W. C., Ram M., Waddington E. D., Mayewski P. A., and Zielinski G. A. (1993) Abrupt increase in Greenland snow accumulation at the end of the Younger Dryas event. *Nature* **362,** 527–529.

Battle M., Bender M., Sowers T., Tans P. P., Butler J. H., Elkins J. W., Ellis J. T., Conway T., Zhang N., Lang P., and Clarke A. D. (1996) Atmospheric gas concentrations over the past century measured in air from firn at the South Pole. *Nature* **383,** 231–235.

Bay R. C., Price P. B., Clow G. D., and Gow A. J. (2001) Climate logging with a new rapid optical technique at Siple Dome. *Geophys. Res. Lett.* **28,** 4635–4638.

Bender M. L., Tans P. P., Ellis J. T., Orchardo J., and Habfast K. (1994a) A high precision isotope ratio mass spectrometry method for measuring the O_2/N_2 ratio of air. *Geochim. Cosmochim. Acta* **58,** 4751–4758.

Bender M. L., Sowers T., Barnola J.-M., and Chappellaz J. (1994b) Changes in the O_2/N_2 ratio of the atmosphere during recent decades reflected in the composition of air in the firn at Vostok Station, Antarctica. *Geophys. Res. Lett.* **21,** 189–192.

Bender M., Sowers T., and Lipenkov V. (1995) On the concentration of O_2, N_2, and Ar in trapped gases from ice cores. *J. Geophys. Res.* **100,** 18651–18660.

Caillon N., Severinghaus J. P., Barnola J.-M., Chappellaz J., Jouzel J., and Parrenin F. (2001) Estimation of Temperature. Change and of Gas Age - Ice Age Difference, 108 kyr BP, at Vostok, Antarctica. *J. Geophys. Res.* **106,** 31893–31901.

Colbeck S. C. (1989) Air movement in snow due to windpumping. *J. Glaciol.* **35,** 209–213.

Craig H. and Wiens R. C. (1996) Gravitational enrichment of $^{84}Kr/^{36}Ar$ ratios in polar ice caps: A measure of firn thickness and accumulation temperature. *Science* **271,** 1708–1710.

Craig H., Horibe Y., and Sowers T. (1988) Gravitational separation of gases and isotopes in polar ice caps. *Science* **242,** 1675–1678.

Cuffey K. M. and Clow G. D. (1997) Temperature, accumulation, and ice sheet elevation in central Greenland through the last deglacial transition. *J. Geophys. Res.* **102,** 26383–26396.

Cuffey K. M., Clow G. D., Alley R. B., Stuiver M., Waddington E. D., and Saltus R. W. (1995) Large arctic temperature change at the Wisconsin-Holocene glacial transition. *Science* **270,** 455–458.

Grachev A. and Severinghaus J. P. (1999) Calibrating the thermal diffusion signal of $^{15}N^{14}N/^{14}N^{14}N$, $^{40}Ar/^{36}Ar$, and $^{18}O^{16}O/^{16}O^{16}O$ for determining the magnitude of abrupt paleotemperature changes. *EOS* **80,** F12 (abstract).

Grachev A. ,and Seveninghous J. P. (2003) Laboratory determination of thermal diffusion constants for $^{29}N_2/^{28}N_2$ in air at temperatures from −60 to 0°C for reconstruction of magnitudes of abrupt climate change using the ice core fossil-air paleothermometer. *Geochim. Cosmochim. Acta* **67,** (3), 345–360.

Grew K. E. and Ibbs T. L. (1952) *Thermal Diffusion in Gases*. Cambridge Univ. Press., New York.

Herron M. M. and Langway C. C. (1980) Firn densification. An empirical model. *J. Glaciol.* **25,** 373–385.

Keeling R. F., Manning A. C., McEvoy E. M., and Shertz S. R. (1998) Methods for measuring changes in atmospheric O_2 concentration and their application in southern hemisphere air. *J. Geophys. Res.* **103,** 3381–3397.

Lang C., Leuenberger M., Schwander J., and Johnsen S. (1999) 16°C rapid temperature variation in central Greenland 70,000 years ago. *Science* **286,** 934–937.

Leuenberger M., Schwander J., and Lang C. (1999) Delta(15)N measurements as a calibration tool for the paleothermometer and gas-ice age differences: A case study for the 8200 BP event on GRIP ice. *J. Geophys. Res.* **104,** 22163–22170.

Manning A. (2001) Temporal variability of atmospheric oxygen from both continuous measurements and a flask sampling network: Tools for studying the global carbon cycle. Ph.D. dissertation, University of California San Diego, La Jolla.

Martinerie P., Raynaud D., Etheridge D., Barnola J.-M., and Mazaudier D. (1992) Physical and climatic parameters which influence the air content in polar ice. *Earth Planet. Sci. Lett.* **112,** 1–13.

McKinney C. R., McCrea J. M., Epstein S., Allen H. A., and Urey H. C. (1950) Improvements in mass-spectrometers for the measurement of small differences in isotope abundance ratios. *Rev. Sci. Instrum.* **21,** 724–730.

Paterson W. S. B. (1969) *The Physics of Glaciers*. Pergamon.

Schwander J. (1989) The transformation of snow to ice and the occlusion of gases. In *The Environmental Record in Glaciers and Ice Sheets* (ed. H. Oeschger and C. C. Langway Jr.), pp. 53–67, John Wiley, New York.

Schwander J., Stauffer B., and Sigg A. (1988) Air mixing in firn and the age of the air at pore close-off. *Ann. Glaciol.* **10,** 141–145.

Schwander J., Barnola J.-M., Andrie C., Leuenberger M., Ludin A., Raynaud D., and Stauffer B. (1993) The age of the air in the firn and the ice at summit, Greenland. *J. Geophys. Res.* **98,** 2831–2838.

Schwander J., Sowers T., Brook E. J., and Bender M. L. (1997) Age scale of the air in the summit ice: Implication for glacial-interglacial temperature change. *J. Geophys. Res.* **102,** 19483–19494.

Severinghaus J. P. and Brook E. J. (1999) Abrupt climate change at the end of the last glacial period inferred from trapped air in polar ice. *Science* **286,** 930–934.

Severinghaus J. P. and Brook E. J. (2000) Do atmospheric gases fractionate during air bubble closure in polar firn and ice? *EOS* **81,** S20 (abstract).

Severinghaus J. P., Sowers T., Brook E. J., Alley R. B., and Bender M. L. (1998) Timing of abrupt climate change at the end of the Younger Dryas period from thermally fractionated gases in polar ice. *Nature* **391,** 141–146.

Severinghaus J. P., Grachev A., and Battle M. (2001) Thermal fractionation of air in polar firn by seasonal temperature gradients. *Geochem. Geophy. Geosy.* vol. 2 (article)**,** 2000GC000146 (2001).

Sowers T., Bender M. L., and Raynaud D. (1989) Elemental and isotopic composition of occluded O_2 and N_2 in polar ice. *J. Geophys. Res.* **94,** 5137–5150.

Sowers T., Bender M. L., Raynaud D., and Korotkevich Y. S. (1992) $\delta^{15}N$ of N_2 in air trapped in polar ice: A tracer of gas transport in the firn and a possible constraint on ice age-gas age differences. *J. Geophys. Res.* **97,** 15683–15697.

Stuiver M., Grootes P. M., and Braziunas T. F. (1995) The GISP2 $\delta^{18}O$ climate. Record of the past 16,500 years and the role of the sun, ocean, and volcanoes. *Quaternary Res.* **44,** 341–354.